الجمهورية الجزائرية الديمقراطية الشعبية
People's Democratic Republic of Algeria
Ministry of Higher Education And Scientific Research
University Abdelhamid Ibn Badis Mostaganem
وزارة التعليم العالي و البحث العلمي
جامعة عبد الحميد بن باديس مستغانم

Faculty of Sciences and Technology
Civil Engineering Department

كلية العلوم و التكنولوجيا
قسم الهندسة المدنية

N° d'ordre : M2/GC/2025

DISSERTATION FOR MASTER'S DEGREE

Field : Civil Engineering
Option : Structures

Topic

STATIC ANALYSIS OF CROSS-PLY LAMINATED PLATES UNDER THERMAL LOADING USING A REFINED DISPLACEMENT

Presented by :

CHIBWE Tanaka Michael

Presented on 18/06/2025 before a jury composed of :

Dr. ELMASCRI Setti	President	University of Mostaganem
Dr. BELBACHIR Nasrine	Supervisor	University of Mostaganem
Dr. ADDOU Farouk Yahia	Examiner	University of Mostaganem

Academic Year 2024/2025

ACKNOWLEDGEMENTS

This dissertation represents the culmination of years of personal effort, perseverance, and continuous learning across different levels of education. I am deeply thankful to God for the grace, strength, and opportunity to reach this significant milestone.

I would like to express my heartfelt gratitude to my supervisor, **Dr. Belbachir Nasrine**, for her invaluable support, guidance, and encouragement throughout this research. Her expertise, dedication, and patience have greatly enriched this work and my academic development.

I also extend my sincere thanks to all the professors of the **Faculty of Science and Technology**, whose teachings laid the foundation for the knowledge and skills that made this work possible.

Furthermore, I would like to express my appreciation to the **members of the jury** for taking the time to review and evaluate this dissertation. Their insights, questions, and recommendations will be of great value to my academic and professional growth.

To everyone who has supported me along this journey, whether through teaching, guidance, or encouragement — thank you.

DEDICATION

All glory and honour be to God, whose grace has brought me this far. His constant presence, guidance, and sustaining power have carried me through every step of this journey.

I dedicate this work:

To my beloved family, whose love and support have been my anchor through every season.

To my parents, Norman and Nomusa Chibwe — thank you for always being there, for your endless sacrifices, and for believing in me. This achievement would not have been possible without your unwavering support.

To my sisters, Chido and Mukudzei Chibwe, for your encouragement, loyalty, and the many ways you've stood by me.

To my uncle, Lucias Chinzvende — I would not be where I am today without the door God opened through you. Your support paved the way for this opportunity.

To Brother Bernard Regis — this work is just as much yours as it is mine. Your selfless help, given freely and sacrificially, has been an extraordinary blessing.

To my friend and brother, Gilbert Mlacha Mwanyika, for walking this academic path with me — your mentorship, prayers, and constant encouragement have made a lasting impact.

To all my friends who have supported me in diverse ways — thank you.

And finally, to my supervisor, Dr. Nasrine Belbachir — thank you for your expertise, dedication, and patient guidance. Your support was key to the completion of this work.

To each of you — thank you for your love, belief, and support. This dissertation is dedicated to you.

CHIBWE Tanaka Michael

ABSTRACT

This study presents the static analysis of cross-ply laminated composite plates under thermal loading using a refined shear deformation theory. Based on Higher-Order Shear Deformation Theory (HSDT), the model incorporates a novel transverse shear function that captures through-thickness warping effects without requiring shear correction factors.

The governing equations were derived using the principle of virtual work and solved analytically through the Navier method. MAPLE 12 was employed for numerical computations. Three laminate configurations ,[0°], [0°/90°], and [0°/90°/0°] were studied under simply supported boundary conditions.

The results from the present theory were compared with those from Classical Plate Theory (CPT), First-Order Shear Deformation Theory (FSDT), HSDT, and the Trigonometric Theory (Ghugal & Kulkarni, 2013), showing strong agreement. Parametric studies explored the effects of aspect ratio (a/h), material anisotropy (E_1/E_2), and thermal expansion coefficient ratio (α_2/α_1) on transverse deflection ($\overline{w}$). It was observed that for [0°/90°] laminates, deflection increased with aspect ratio, while for [0°/90°/0°], it decreased. Deflection decreased with increasing material anisotropy and increased with thermal expansion coefficient ratio.

The proposed model proves accurate and efficient for analyzing laminated composite plates, offering valuable insights for the design of thermally loaded composite structures.

Keywords:

Laminated Composite Plates, Refined Shear deformation theory, Thermal Loading, Deflection, Stresses, Navier solution, Thermal Expansion, Aspect Ratio, Material Anisotropy.

RÉSUMÉ

Cette étude présente l'analyse statique des plaques composites stratifiées croisées sous chargement thermique en utilisant une théorie de déformation de cisaillement raffinée. Basé sur la théorie de déformation par cisaillement d'ordre supérieur (HSDT), le modèle intègre une fonction de cisaillement transverse innovante qui prend en compte les effets de gauchissement selon l'épaisseur sans nécessiter de facteurs de correction de cisaillement.

Les équations gouvernantes ont été dérivées à l'aide du principe des travaux virtuels et résolues analytiquement par la méthode de Navier. Le logiciel MAPLE 12 a été utilisé pour les calculs numériques. Trois configurations de stratification, [0°], [0°/90°] et [0°/90°/0°], ont été étudiées sous des conditions aux limites simplement appuyées.

Les résultats obtenus avec la théorie proposée ont été comparés à ceux issus de la théorie classique des plaques (CPT), de la théorie de déformation par cisaillement d'ordre un (FSDT), de la HSDT et de la théorie trigonométrique (Ghugal & Kulkarni, 2013), montrant une forte concordance. Des études paramétriques ont examiné les effets du rapport d'aspect (a/h), de l'anisotropie du matériau (E_1/E_2), et du rapport des coefficients de dilatation thermique (α_2/α_1) sur la flèche transverse ($\overline{w}$). Il a été observé que, pour les stratifiés [0°/90°], la flèche augmentait avec le rapport d'aspect, tandis que pour les stratifiés [0°/90°/0°], elle diminuait. La flèche décroissait avec l'augmentation de l'anisotropie du matériau et augmentait avec le rapport des coefficients de dilatation thermique.

Le modèle proposé s'est révélé précis et efficace pour l'analyse des plaques composites stratifiées, offrant des perspectives précieuses pour la conception de structures composites soumises à des chargements thermiques.

Mots-clés :

Plaques composites stratifiées, Théorie de déformation de cisaillement raffinée, Chargement thermique, Flèche, Contraintes, Solution de Navier, Dilatation thermique, Rapport d'aspect, Anisotropie du matériau.

LIST OF NOTATIONS

G	Shear Modulus (x, z)
ν	Poisson's Ratio (x, z)
E	Young's Modulus
a	Length of the plate
b	Width of the plate
h	Thickness of the plate
u, v, w	Displacements in the x, y, z directions
u_0, v_0, w_0	Mid-plane displacements in the x, y, z directions respectively
σ_{ij}	Stress Tensor
ε_{ij}	Strain Tensor
$\sigma_{xx}, \sigma_{yy}, \sigma_{zz}$	Normal stresses in the x ,y ,z directions respectively
$\varepsilon_{xx}, \varepsilon_{yy}, \varepsilon_{zz}$	Normal strains in the x ,y ,z directions respectively
τ_{xy}	In-plane shear stress
τ_{yz}, τ_{xz}	Transverse shear stresses
$\varepsilon^0_{xx}, \varepsilon^0_{yy}, \gamma^0_{xy}$	In-plane mid-plane strains
θ_x, θ_y	High-Order Shear rotations
C_{ij}	Stiffness Tensor
ϕ_x, ϕ_y	Rotations about the y- and x-directions respectively
Q_{ij}	Stiffness coefficient in the local coordinate system
$\bar{Q}_{ij}$	Stiffness coefficient in the global coordinate system
U	Strain Energy
V	Work of external forces
N_{xx}, N_{yy}	Normal forces in the x ,y directions respectively
M_{xx}, M_{yy}	Bending moment resultants per unit length

γ_{xz}, γ_{yz}	Transverse Shear Strains
γ_{xy}	In-plane Shear Strain
$\gamma_{xz}^{0}, \gamma_{yz}^{0}$	Mid-plane transverse shear strains
$\delta u, \delta v, \delta w, \delta\theta_x, \delta\theta_y$	Virtual Displacements
∂	Partial Derivative
$f(z)$	Transverse Shear Function
M_{xy}	In-plane twisting moment per unit length
N_{xy}	In-plane shear force per unit length
[A]	Membrane/extensional stiffness matrix
[B]	Membrane-Bending Coupling Matrix
[D]	Bending stiffness matrix
α_x, α_y	Coefficients of thermal expansion in x and y directions respectively
$A_{ij}, B_{ij}, D_{ij}, E_{ij}, F_{ij}, H_{ij}$	Laminate Stiffness Coefficients
T	Thermal Load
q	Load
[K]	Stiffness Matrix
$\{F\}$	Force Vector
$\{\Delta\}$	Generalized Displacement Vector
$i ; j$	Natural Numbers
$\{\ \}$	Column Vector
$[\ ]$	Matrix

LIST OF FIGURES

LIST OF TABLES

TABLE OF CONTENTS

GENERAL INTRODUCTION

In modern engineering, laminated composite materials are increasingly preferred for structural applications due to their high strength-to-weight ratio, corrosion resistance, and customizable mechanical properties. Cross-ply laminated plates, in particular, are widely used in aircraft panels, ship hulls, automotive components, and civil structures. These plates are frequently subjected to thermal loads, making their accurate analysis essential for safe and reliable design.

Traditional plate theories such as the Classical Plate Theory (CPT) and First-Order Shear Deformation Theory (FSDT) provide simplified tools for analyzing such structures. However, these models fall short in capturing transverse shear deformation and through-thickness warping effects, especially in thick and moderately thick laminates. While Higher-Order Shear Deformation Theories (HSDTs) address some of these limitations, many existing formulations still rely on shear correction factors and simplified assumptions that reduce accuracy under complex loading.

PROBLEMATIC

Despite progress in plate theories, accurately predicting the static response of laminated composite plates under thermal loading remains a challenge. Most analytical models either neglect thermal effects or treat them simplistically, leading to underestimation or misrepresentation of deformations and stress distributions. Furthermore, the lack of refined models that incorporate realistic shear behavior without correction factors limits the practical applicability of many classical approaches. These limitations highlight the need for a more precise and efficient analytical model that accounts for thermal loads in cross-ply laminates.

This study addresses these challenges by applying a refined displacement field developed by (Mantari et al., 2012), based on Higher-Order Shear Deformation Theory (HSDT), which includes a novel transverse shear function. The model enables accurate analysis of laminated composite plates without requiring shear correction factors. The governing equations are derived using the principle of virtual work and solved analytically using the Navier method under simply supported boundary conditions.

By comparing results with existing theories and exploring the influence of various parameters, this dissertation aims to contribute to the development of more reliable and accurate models for the static analysis of laminated composites under realistic service conditions.

Chapter 1

GENERAL INFORMATION ON COMPOSITE MATERIALS

1.1. Introduction

In a world that is constantly evolving, the demand for materials that are lightweight, strong, and adaptable has led to the adoption of composite materials. These advanced materials are formed by combining two or more distinct materials on a macroscopic scale—typically a matrix and reinforcement—to achieve enhanced mechanical, thermal, and functional properties. Composite materials offer a unique balance of strength, weight, and durability, making them highly desirable across various industries. Their properties can be easily tailored by adjusting fiber type, matrix composition, fiber orientation, and layer arrangement, allowing engineers to design materials for specific applications.

Because of their versatility in design and functionality, composite materials can be fabricated into complex shapes and customized dimensions, making them suitable for applications requiring high strength-to-weight ratios, impact resistance, and environmental durability. Depending on their composition, they serve as primary structural elements capable of withstanding mechanical stress, shock, and vibration, or as secondary functional components providing insulation against heat, sound, and electricity. These qualities have positioned composites as key materials in the aerospace, automotive, construction, biomedical, and energy sectors. As industries push for greater efficiency and innovation, composites are set to redefine the future of engineering and material design.

This chapter provides a comprehensive overview of composite materials, including their classification, properties, structural architecture, and applications. Understanding these fundamental concepts is crucial to appreciating their growing role in modern technology and industry.

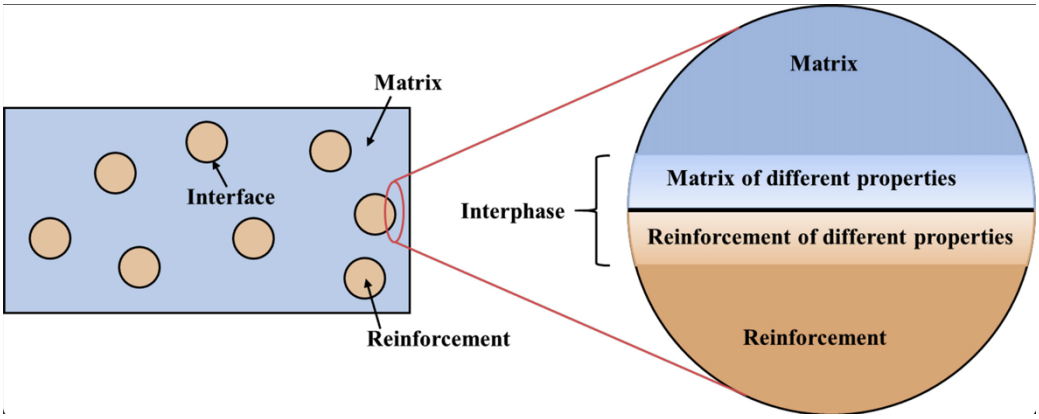

Figure 1:Constituents of Composite Materials

1.2. Constituents of Composite Materials

A composite material consists of two or more chemically distinct constituents, separated by a distinct interface that differentiates the reinforcing particle from the matrix. It exhibits a unique combination of properties that are noticeably different from those of its individual constituents. Typically, the discontinuous phase (reinforcement) is embedded within the continuous phase (matrix) (Chawla, 2012; Mallick, 2007; Yi & Du, 2011).

1.2.1. Matrix

The matrix is a continuous, uniform material that embeds the fiber system of a composite. It binds and holds the reinforcements together, forming a solid structure. In addition to providing structural integrity, the matrix also protects the reinforcements from environmental damage, facilitates load transfer, and contributes to the composite's overall texture, durability, and appearance (Mallick, 2007; Altenbach & Kissing, 2004). The matrix also plays a key role in enhancing long-term environmental stability and interfacial adhesion with fibers (Foreman, 2005; Harris, 1999). The selection of matrix material depends on the intended application and required performance characteristics such as mechanical strength, thermal resistance, and weight. Matrix materials are typically classified into three main types, each suitable for specific operational environments (Baker, Dutton & Kelly, 2004; Brigante, 2014).

Types of Matrices:

- Polymer Matrices ,
- Metal Matrices , and
- Ceramic Matrices .

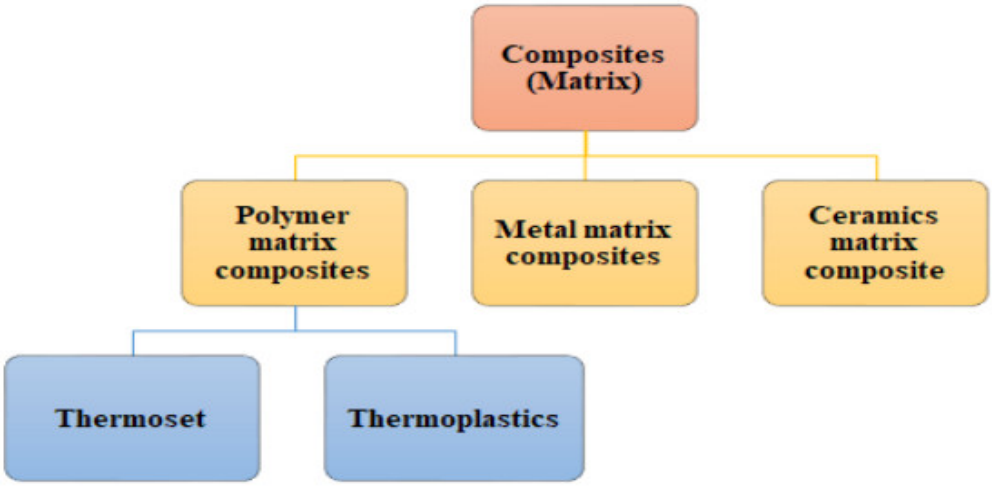

Figure 2:Classification of Composites based on Matrix type

a. Polymer Matrix

The polymer matrix is the most widely used category in composite materials, primarily due to its lightweight characteristics, ease of processing, and cost-effectiveness. It acts as the continuous phase that binds the reinforcing fibers together and facilitates the transfer of loads between them (Mallick, 2007; Chawla, 2012). Polymer matrix composites (PMCs) are typically categorized into two types based on the resin system used: thermosets and thermoplastics. Each offers distinct advantages in terms of processing and performance, making them suitable for a wide range of structural and functional applications (Herakovich, 1998; Altenbach et al., 2015).

i. Thermosets

Thermosets are materials that undergo a chemical transformation, known as curing, during which they typically change from a liquid to a solid state. In their uncured form, they consist of small, unlinked molecules called monomers. When a cross-linker, curing agent, catalyst, or an external influence like heat is introduced, a chemical reaction is triggered. This reaction causes the monomers to form longer molecular chains and a cross-linked network, resulting in solidification. This transformation is permanent and irreversible (Chawla, 2012; Yi & Du, 2011). Once cured, exposing thermosets to high temperatures does not cause them to melt—instead, they degrade.

Thermosets are more predominantly used as matrix materials in structural composites due to their superior stiffness and thermal resistance (Brigante, 2014; Altenbach & Altenbach, 2010). Common types include epoxy, polyester, phenolic resins, and polyimides.

- ***Polyester***

Polyester resins are highly versatile due to their ability to be modified or customized during polymer chain formation. This adaptability has made them valuable across nearly all areas of the composites industry. Their primary advantage lies in offering a well-balanced combination of properties—including mechanical strength, chemical and electrical resistance, dimensional stability, and ease of processing (Mallick, 2007; NATO Science Series, 2001). According to Zhang and Du (2010), their relatively low cost also makes them suitable for large-volume structural applications.

Figure 3:Polyester Resins

- ***Epoxy***

Epoxy resins are widely used in composite parts, structural components, and concrete repair due to their excellent mechanical properties, low shrinkage, and high chemical resistance (Baker, Dutton & Kelly, 2004). Their structure can be tailored to produce different performance characteristics. Compared to unsaturated polyesters, epoxy resins shrink less during curing and exhibit superior adhesion to fiber reinforcements (Foreman, 2005). However, they are sensitive to UV degradation, which limits their outdoor performance unless stabilized (Harris, 1999; Brigante, 2014).

Figure 4:Epoxy Resins

- ***Phenolic Resins***

Phenolic resins, derived from phenol, are thermosetting polymers that cure through condensation reactions, during which water is released. Composites using phenolic matrices demonstrate excellent fire resistance, low smoke emission, sound absorption, and corrosion

resistance (Herakovich, 1998; Altenbach & Kissing, 2004). These characteristics make them ideal for applications in aerospace interiors, public transportation, and industrial insulation systems (Zhang & Du, 2010).

- ***Polyimides***

Polyimides are high-performance polymers used in extreme thermal environments. They offer better flame resistance and mechanical property retention at elevated temperatures than most conventional thermosets (Chawla, 2012; Brigante, 2014). However, their limitations include low fracture toughness and brittleness, which can restrict use in impact-sensitive components (Altenbach et al., 2015; NATO Science Series, 2001).

ii. Thermoplastics

Thermoplastics are a class of melt-processable polymers that can be repeatedly softened and reshaped through the application of heat. When the temperature of a thermoplastic material is raised above its melting point, it transitions into a softened or liquid state suitable for processing. Upon cooling below this temperature, it resolidifies into a glass-like solid. This reversible phase change allows thermoplastics to be reprocessed multiple times; however, repeated heating can lead to thermal degradation, gradually reducing the material's performance and mechanical properties (Foreman, 2005; Brigante, 2011). Many thermoplastic polymers are addition-type polymers, capable of forming extremely long molecular chains or achieving high molecular weights, which contribute to their strength and versatility across a wide range of applications (Yi & Zhang, 2006; Herakovich, 1998).

Common examples of thermoplastic resins include polyethylene, polystyrene, nylon (polyamide), polycarbonate, polysulfone, polyphenylene sulfide (PPS), and acrylonitrile-butadiene-styrene (ABS), among others (Harris, 1999).

- ***Polyethylene***

Polyethylene (PE) is a translucent thermoplastic known for its adequate mechanical strength, flexibility across a broad temperature range, and excellent resistance to corrosion, making it suitable for a wide variety of applications. The primary types of polyethylene include Low-Density Polyethylene (LDPE) and High-Density Polyethylene (HDPE) (Altenbach & Altenbach, 2004).

- ***Polystyrene***

Polystyrene is a clear, odorless, and tasteless thermoplastic that is widely used in various applications. In its pure form, it is relatively brittle, which limits its use in impact-prone environments. However, its impact resistance can be significantly enhanced through copolymerization with polybutadiene rubber, resulting in high-impact polystyrene (HIPS). Polystyrene also exhibits good dimensional stability and low curing shrinkage, making it suitable for precision-molded products and applications requiring consistent geometrical properties (Dutton & Kelly, 2004; NATO Science Series, 2001).

- ***Polyamides (Nylons)***

Polyamides, commonly known as nylons, are a class of thermoplastic polymers distinguished by the presence of repeating amide (-CONH-) linkages in their main-chain molecular structure. These materials exhibit high tensile strength, good toughness, and excellent chemical resistance, making them highly suitable for demanding engineering applications (Du, 2002; Kissing, 2003).

b. Metal Matrix

In metal matrix composites (MMCs), a metal acts as the continuous matrix phase, embedding reinforcement elements such as ceramic particles, fibers, or whiskers. The matrix provides structural support and facilitates the effective transfer of stress between the matrix and the reinforcement, thereby enhancing the overall mechanical and thermal properties of the composite (Chawla, 2012; Zhang, 2008).

Metal matrices are particularly valued in high-temperature environments where polymer matrices fail to perform. Unlike polymers, metals can retain their strength and stiffness under thermal and mechanical stress. Additionally, metal matrices offer superior thermal conductivity, wear resistance, and corrosion resistance (Miracle, 2005; Brigante, 2011; Herakovich, 1998).

The most commonly used metal matrices include:

- Aluminum, known for its low density and corrosion resistance (Clyne & Withers, 1993);
- Magnesium, which is even lighter and often used where weight savings are critical (Du, 2002);

- Titanium, favored for its high strength-to-weight ratio and corrosion resistance (Baker et al., 2004);
- Nickel and cobalt alloys, used in high-temperature applications such as turbine engines and aerospace components (Surappa, 2003; Altenbach & Kissing, 2005).

Compared to polymer or ceramic matrices, metal matrices offer a more balanced combination of mechanical toughness and thermal performance. While ceramics can withstand extreme temperatures, they are brittle; polymers, though tough and easy to process, degrade under heat. Metal matrices, in contrast, provide a middle ground with good ductility, strength, and thermal stability (Strong, 2008; NATO Science Series, 2001).

c. Ceramic Matrix

When operating temperatures exceed 1000°C, traditional materials like polymers and metals begin to fail due to thermal degradation, oxidation, and loss of mechanical integrity. In such conditions, Ceramic Matrix Composites (CMCs) provide a superior alternative because of their thermal stability, oxidation resistance, and high structural integrity under extreme environments (Chawla, 2012; Yi, 2003). These composites typically consist of a ceramic matrix such as silicon carbide (SiC), alumina (Al_2O_3), or zirconia (ZrO_2), reinforced with ceramic fibers or whiskers like SiC or alumina fibers, which help overcome the inherent brittleness of monolithic ceramics (Du & Zhang, 2000; Brigante, 2011).

The synergy between the matrix and the reinforcement provides improved fracture toughness, thermal shock resistance, and load-bearing capability, making CMCs suitable for high-demand environments including gas turbine engines, hypersonic vehicles, nuclear reactors, and thermal protection systems (Clyne & Withers, 1993; NATO Science Series, 2000; Altenbach et al., 2013). Furthermore, ceramic matrices exhibit low thermal conductivity, excellent wear resistance, and chemical inertness, critical for resisting oxidation and corrosion at elevated temperatures (Strong, 2008; Berthelot, 1999).

Nevertheless, the manufacturing of CMCs remains technically complex and resource-intensive, often involving methods like chemical vapor infiltration (CVI), liquid phase infiltration, or hot pressing. These processes can introduce porosity, residual stresses, or interface challenges, which must be carefully controlled to optimize performance (Gay & Hoa, 2007; Kissing, 2010). Despite these challenges, their unmatched performance under harsh conditions ensures their continuing application in advanced structural and functional systems (Surappa, 2003; Foreman, 2005).

1.2.2. Reinforcement

In composite materials, the reinforcement phase serves as the principal load-carrying component, dramatically enhancing the mechanical, thermal, and fatigue properties of the structure. While the matrix distributes stress and protects the reinforcements, it is the reinforcement material that contributes most significantly to strength, stiffness, and durability (Chawla, 2012; Mallick, 2007; Harris, 1999). The reinforcement's performance depends on parameters such as type, orientation, aspect ratio, volume fraction, and the matrix-reinforcement interface quality (Herakovich, 1997; Callister & Rethwisch, 2014).

Types of Reinforcements:

- Fiber Reinforcements
- Particulate Reinforcements
- Flake or Platelet Reinforcements

a. Fiber Reinforcements

Fiber reinforcements are the most widely used and are classified based on their length, alignment, and type.

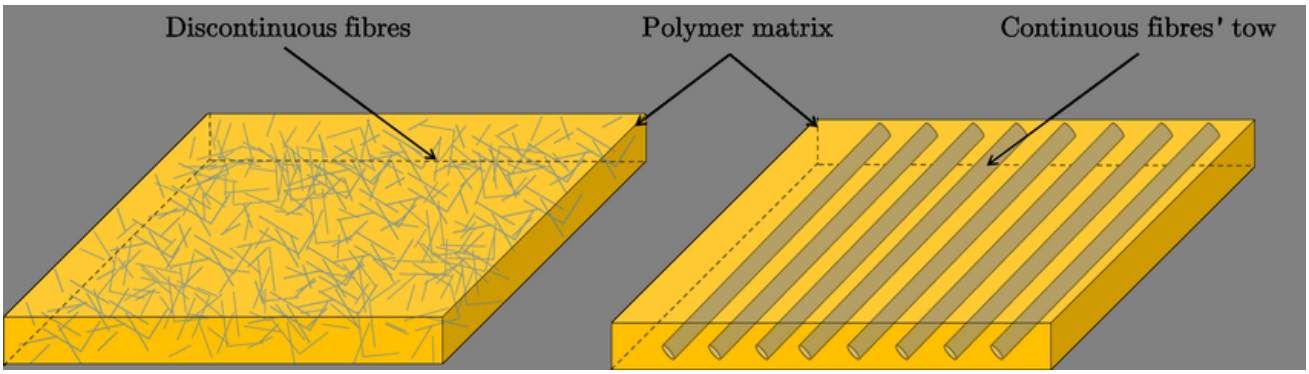

Figure 5:Discontinuous and Continuous Fibers in Polymer Matrix

i. Continuous Fibers

Continuous fibers run along the full length of the composite component, allowing for optimal load transfer and minimum fiber-matrix discontinuity. These are often used in structural applications where high unidirectional strength is needed, such as aerospace skins, wind turbine blades, and automotive chassis parts (Baker et al., 2004; Berthelot, 1999).

- ***Carbon Fibers***

Carbon fibers are highly sought after due to their low density, outstanding tensile strength, and superior fatigue and corrosion resistance. Derived primarily from polyacrylonitrile (PAN) or pitch precursors, they are used extensively in aerospace, defense, motorsports, and civil structures requiring light weight and high performance (Chawla, 2012; Berthelot, 1999). Moreover, their tailorable modulus, depending on the heat treatment process, offers versatility for both rigid and flexible designs (Zhang & Du, 2000; Harris, 1999; Altenbach & Altenbach, 2004).

- ***Glass Fibers***

Glass fibers remain a cost-effective and widely used reinforcement option. Their moderate tensile strength, good fatigue resistance, and excellent corrosion resistance make them popular in construction, automotive, marine, and sporting goods (Strong, 2008; Callister & Rethwisch, 2014; Dutton & Kelly, 1998). When used with polymer matrices, they form Glass Fiber-Reinforced Polymers (GFRPs), known for their design flexibility, dimensional stability, and low cost (Foreman, 2005; Herakovich, 1997). Their low density (~2.5 g/cm³) also contributes to weight-sensitive structural designs (Brigante, 2011).

Figure 6:Fiber Glass

- ***Aramid Fibers***

Aramid fibers, such as Kevlar® and Twaron®, are valued for their impact resistance, abrasion tolerance, and light weight. These aromatic polyamides are typically used in body armor, aerospace components, and automotive crash structures, where energy absorption is critical (Mallick, 2007; Chung, 2010; Berthelot, 1999). While aramids offer excellent tensile properties

along the fiber axis, they are sensitive to UV exposure and moisture, requiring careful protective measures (Gay & Hoa, 2007; Yi, 2003). Their fatigue resistance also makes them suitable for cyclically loaded components.

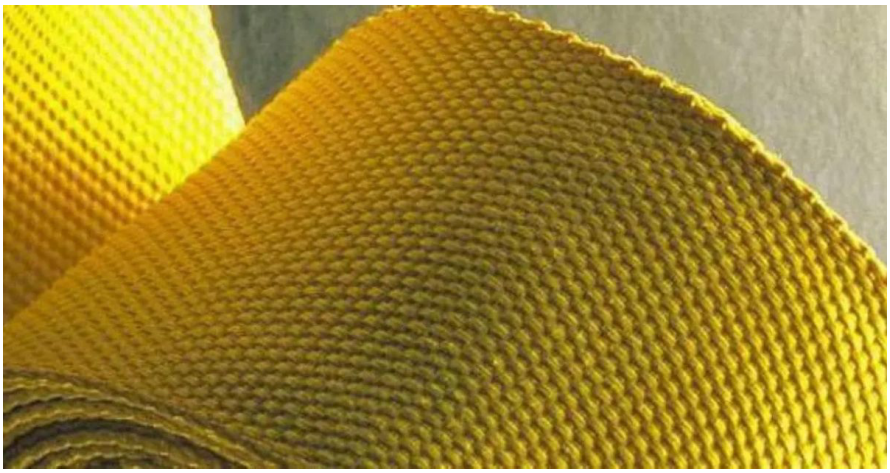

Figure 7:Aramid fibers

ii. Discontinuous Fibers

Discontinuous fibers, also known as short fibers, are small fragments of reinforcing material used in composite structures. Unlike continuous fibers that run through the entire length of a composite, these fibers are shorter and usually scattered randomly or partially aligned within the matrix. Their short length makes them ideal for manufacturing processes such as injection and compression molding, especially when complex shapes are required.

Although they do not provide as much strength or stiffness as continuous fibers, they still improve the mechanical performance of the material compared to an unreinforced matrix. Their effectiveness depends on factors like fiber length, orientation, volume fraction, and the quality of the bond with the matrix. Short fiber composites are especially useful in applications where moderate strength, low cost, and easy processing are more important than maximum performance (Yi et al., 2006; Chawla, 2012; Brigante, 2014).

b. Particulate Reinforcements

Particulate reinforcements are small, usually round or irregular particles added to a matrix to improve its properties. Unlike fibers, which mainly enhance strength in specific directions, particles strengthen the material in all directions. These particles can be made of ceramics, metals, or polymers and are often used in metal or polymer matrices.

Particulates help increase the stiffness, wear resistance, and sometimes strength of the composite without greatly increasing the cost or making the manufacturing process more difficult. They are widely used in structural and wear-resistant applications (Callister & Rethwisch, 2014; Altenbach & Altenbach, 2004; Foreman, 2011).

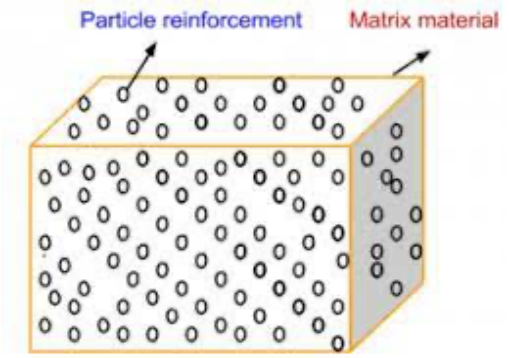

Figure 8:Particle Reinforcement in a Matrix Material

c. Flake or Platelet Reinforcements

Flake or platelet reinforcements are flat, thin particles with a large surface area compared to their thickness. When added to a matrix, these reinforcements can improve the composite's resistance to gas or moisture, increase thermal or electrical conductivity, and provide better dimensional stability.

Common materials used for flakes include graphite, glass, mica, and aluminum. These reinforcements are particularly effective when aligned parallel to the composite surface, forming layers that help block heat, gas, or crack propagation. This makes them suitable for applications such as coatings, packaging, and heat dissipation components in electronics (Strong, 2008; Zhang, 2009; Gay & Hoa, 2007).

While flakes do not provide as much tensile strength as fibers, they can help absorb energy and slow down crack growth, which improves durability (Harris, 1999; Herakovich, 1998; NATO Science Series, 2003).

1.2.3. Interface / Bonding

In composite materials, the interface is the region where the reinforcement comes into contact with the matrix. This area plays a crucial role in determining the overall performance of the composite. A strong bond at the interface allows efficient load transfer from the matrix to the reinforcement, which improves properties such as tensile strength, fatigue resistance, and impact performance (Callister & Rethwisch, 2014; Mallick, 2007; Herakovich, 1998).

Bonding at the interface can occur through different mechanisms, including mechanical interlocking, chemical adhesion, interdiffusion, and electrostatic forces. In fiber-reinforced composites, treatments like fiber sizing or surface modification are often applied to improve this interaction. These processes enhance adhesion and help prevent defects such as debonding, cracking, or delamination under load (Bledzki & Gassan, 1999; Pickering, 2008; Du & Zhang, 2013).

Several factors influence the quality of interfacial bonding. These include the surface roughness of the reinforcement, chemical compatibility between phases, and the processing methods used. For example, high-temperature processing may improve fiber wetting, but it can also create residual thermal stresses that weaken the bond over time (Facca et al., 2006; Berthelot, 1999; NATO Science Series, 2003).

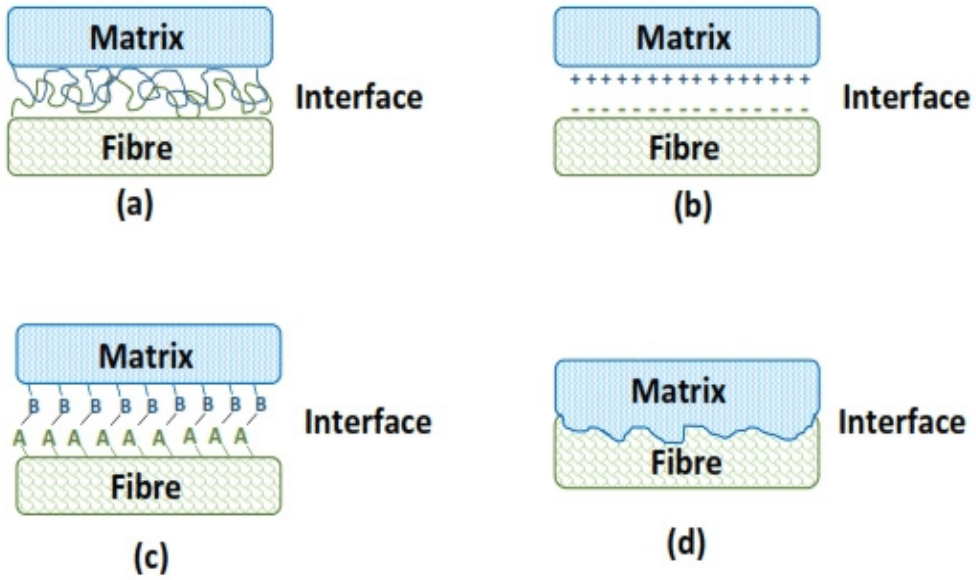

Figure 9:Fiber-Matrix Interface bonding mechanisms.(a) Interdiffusion; (b)electrostatic adhesion; (c)chemical bonding; (d)mechanical interlocking

1.3. Structure (Architecture) of Composites

The internal structure, or architecture, of composite materials plays a key role in determining their mechanical performance under different loading conditions. Depending on how the fibers and matrix are arranged, composites are typically categorized into three main types: monolayers, laminates, and sandwich structures. Each type has distinct features and is suited to different applications based on its mechanical properties.

1.3.1. Monolayer Composites

A monolayer, or lamina, is a single layer of composite material where fibers are aligned in one direction within the matrix. This alignment gives excellent strength and stiffness along the fiber direction, but reduced performance in the transverse direction. Monolayers form the basic building blocks for more complex structures like laminates (Mallick, 2007; Reddy, 2004).

In thin monolayers, behavior is predictable and easier to model. However, as thickness increases, fiber-matrix interactions become more complex, requiring more advanced analysis methods (Chawla, 2012; Kissing & Dutton, 2003).

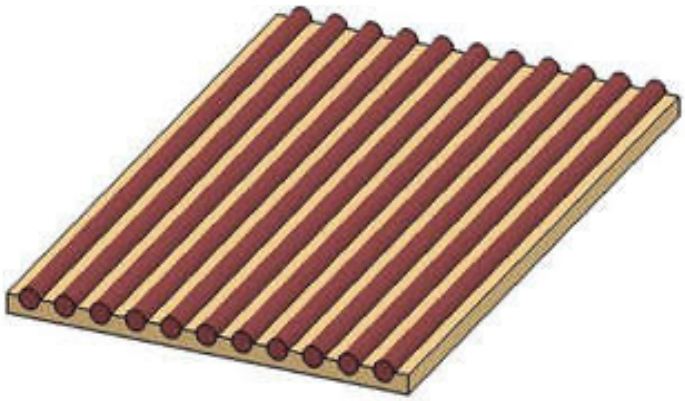

Figure 10:Monolayer composite with reinforcement(fibers)

1.3.2. Laminated Composites

Laminated composites are created by stacking multiple monolayers with varying fiber orientations (e.g., 0°, ±45°, 90°). This design helps distribute loads more efficiently and tailor mechanical properties to specific applications. For example, fibers aligned at 0° resist axial loads, ±45° layers resist shear, and 90° layers improve stiffness across the width (Jones, 1999; Reddy, 2004; Zhang & Yi, 2006).

Laminates are often arranged in specific stacking sequences, like [0/±45/90]s, to reduce warping, enhance stiffness, and improve damage tolerance. The design of laminates requires consideration of layer interactions, residual stresses, and the possibility of delamination under fatigue or impact loads (Gay & Hoa, 2007; Dutton et al., 2004; Altenbach & Altenbach, 2004).

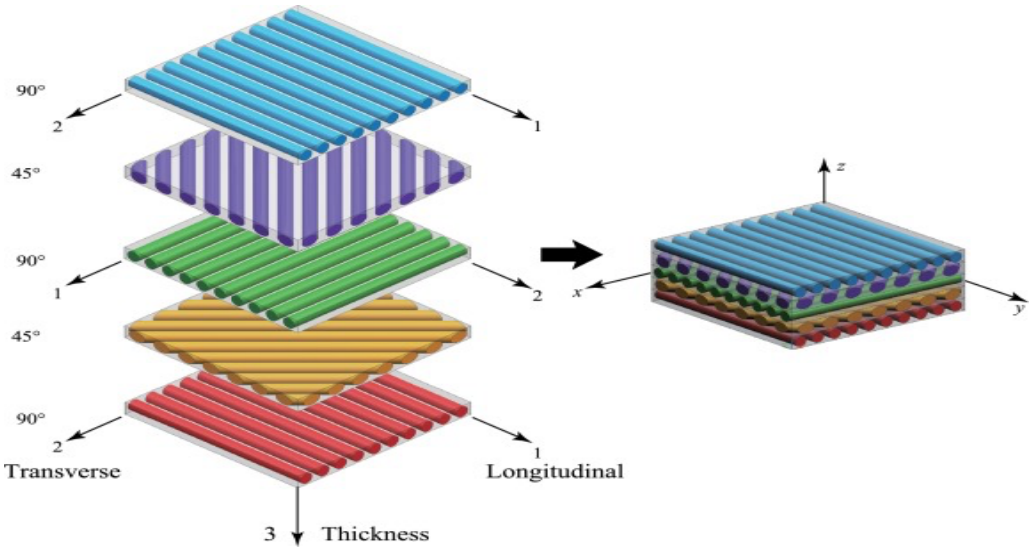

Figure 11:Laminated Composite showing different fiber orientations

1.3.3. Sandwich Composites

Sandwich composites consist of two strong face sheets and a lightweight core material in between. The face sheets carry most of the bending load, while the core resists shear forces and helps maintain the structural shape. This configuration results in a high strength-to-weight ratio, making sandwich structures suitable for aerospace, marine, and automotive applications (Allen, 1969; Reddy, 1997).

Typical core materials include foam, honeycomb structures, or lightweight woods such as balsa. These cores are selected for their low density and ability to absorb shear forces without adding much weight. However, differences in stiffness between the face sheets and the core must be managed carefully to avoid stress concentrations and failure at the interface (Foreman, 2011; Harris, 1999; Brigante, 2014).

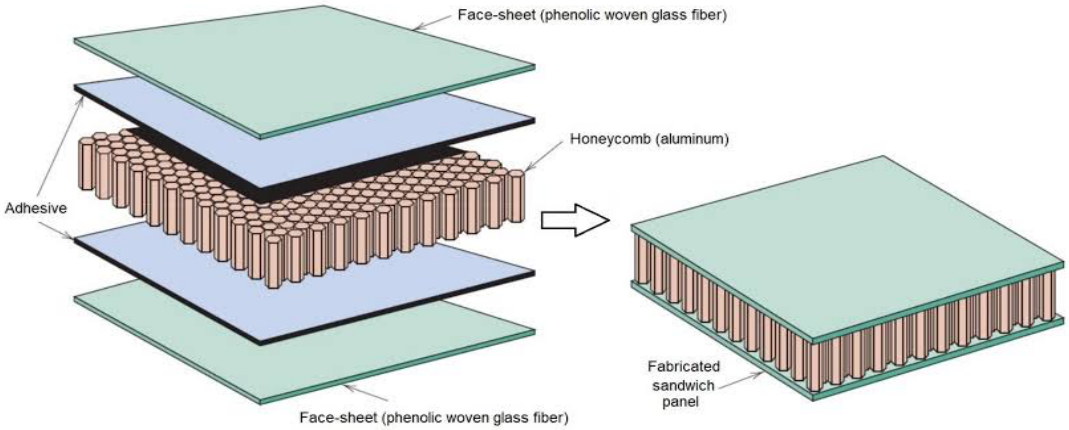

Figure 12:Sandwich Composite

1.4. Domain of Application of Composites

Composite materials are widely used across various industries due to their high strength-to-weight ratio, durability, and resistance to corrosion and environmental degradation. Though initially developed for aerospace use, their applications now extend to civil infrastructure, automotive systems, marine structures, wind energy, and sports equipment. This growing use reflects the need for high-performance, lightweight alternatives to traditional materials (Gay & Hoa, 2007; Chawla, 2012; Altenbach & Altenbach, 2004).

1.4.1. Aerospace Applications

The aerospace industry has led the development and use of composites due to its need for components that are light, strong, and resistant to fatigue. Carbon fiber-reinforced polymers (CFRPs) are widely used in aircraft wings, fuselage parts, and braking systems, while ceramic matrix composites are ideal for high-temperature areas like jet engines (Kaw, 2005; Daniel & Ishai, 2006; Berthelot, 1999).

Composites allow engineers to customize material properties for different aircraft parts, improving both fuel efficiency and structural performance. Sandwich structures and laminated composites are particularly important in modern aerospace design for their ability to balance weight, stiffness, and strength (Baker, Dutton & Kelly, 2004; NATO Science Series, 2003).

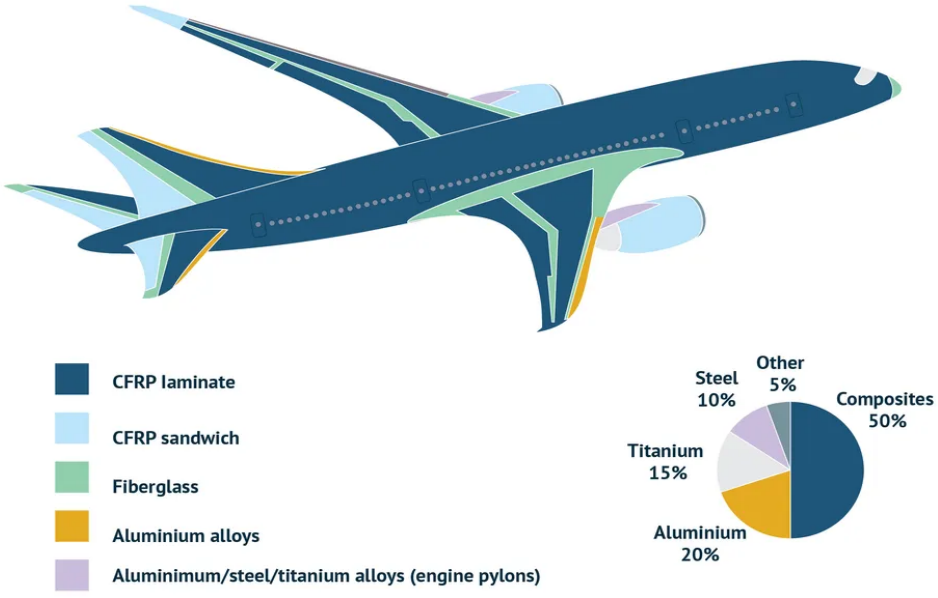

Figure 13:Use of Composite Materials in Aeronautics Field

1.4.2. Automotive Industry

In the automotive sector, composites are increasingly used to enhance fuel efficiency, safety, and overall performance. Their light weight helps reduce vehicle mass, which in turn improves fuel economy and lowers emissions. These materials are used in body panels, bumpers, dashboards, and even under-the-hood components (Mallick, 2007; Dutton et al., 2004).

Composites also offer design freedom, corrosion resistance, and improved crash performance. They are increasingly used in public and emergency vehicles like buses and ambulances for their ability to combine durability and lightweight construction (Zhang & Yi, 2006; Brigante, 2014; Foreman, 2011).

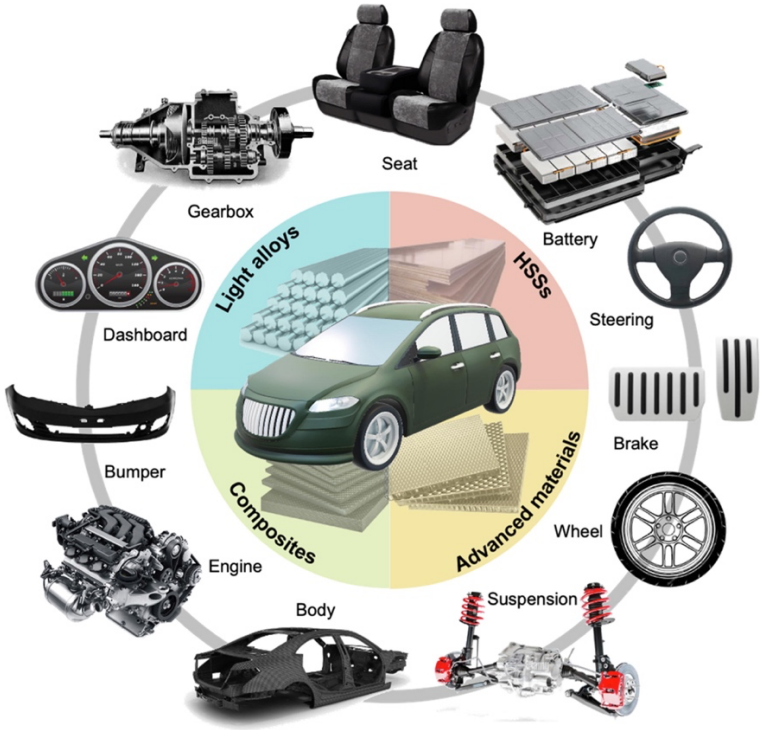

Figure 14:Application of Composites in Automotive Industry

1.4.3. Agriculture

In agriculture, composites are valued for their strength, durability, and resistance to moisture and chemicals. They are used in machinery such as tractors and harvesters, and in stationary systems like silos, tanks, and irrigation components. Their resistance to harsh weather and chemicals makes them ideal for long-term use in outdoor farming environments (Pickering, 2015; Herakovich, 1998; Du & Zhang, 2013).

1.4.4. Marine and Nautical Applications

Marine environments demand materials that can withstand corrosion, UV exposure, and high loading. Composites meet these needs and are widely used in boat hulls, decks, and other structural parts. They are employed in a variety of vessels, including recreational boats, military ships, and commercial fishing craft (Mouritz & Gibson, 2006; Harris, 1999).

Their light weight improves buoyancy and speed, while their corrosion resistance extends service life. The use of foam and honeycomb cores in marine sandwich structures also improves strength without adding bulk (Baker et al., 2004; Kissing & Dutton, 2003).

Figure 15:Use of Composites in Marine Industry

1.4.5. Civil Engineering and Construction

Fiber-reinforced polymer (FRP) composites are being used to repair, retrofit, and reinforce concrete structures. Carbon fiber composites are especially effective in improving the load-bearing capacity of beams, slabs, and columns. These materials are also valued for their resistance to corrosion and ease of installation (Hollaway, 2010; ACI Committee 440, 2015).

They offer an alternative to steel reinforcements, particularly in bridges, tunnels, and buildings requiring seismic upgrades. Composites in construction reduce maintenance costs and extend the life of infrastructure (Gay, 2007; Altenbach & Altenbach, 2004; Berthelot, 1999).

Figure 16:Repair and rehabilitation of corroded bridge & RC columns with FRP Composites (Mosallam,2014).

1.5. Advantages and Disadvantages of Composite Materials

Composite materials offer a variety of benefits across many industries. However, they also come with some limitations that must be considered in their application. Below is an overview of the main advantages and disadvantages of composites.

1.5.1. Advantages

a. High Strength-to-Weight Ratio:

Composites are much lighter than metals while offering comparable or superior strength. This makes them ideal for aerospace, automotive, and marine applications where weight reduction is crucial (Mallick, 2007; Herakovich, 1998; Chawla, 2012).

b. Design Flexibility:

Composites can be shaped into complex geometries that are difficult to produce using conventional materials. This supports innovation in product design across industries (Ashby, 2011; Gay & Hoa, 2007; Brigante, 2014).

c. Corrosion Resistance:

Composites resist corrosion from moisture, salt, and chemicals, making them suitable for marine, automotive, and agricultural environments (Jones, 2013; Zhang & Yi, 2006; Foreman, 2011).

d. Fatigue and Wear Resistance:

Many composites can endure repeated loading without significant degradation. This property is crucial in high-performance uses like turbine blades, car suspensions, and aircraft wings (Mallick, 2007; Altenbach & Altenbach, 2004).

e. Tailored Properties:

By changing the type and orientation of fibers and matrices, composites can be tailored for specific strength, stiffness, thermal, or electrical properties. This versatility allows engineers to fine-tune materials to meet complex demands (Chawla, 2012; Daniel & Ishai, 2006; Gay, 2007).

1.5.2. Disadvantages

a. High Manufacturing Costs:

Producing composite components often requires specialized tools, long curing times, and skilled labor, making them more expensive than metals or plastics (Mallick, 2007; Berthelot, 1999).

b. Difficult to Repair:

Unlike metals, composites don't easily show surface damage, and internal cracks like delamination may be hidden. Repairs often require expertise and specialized materials (Ashby, 2011; Brigante, 2014).

c. Sensitivity to Impact Damage:

Although strong under normal loading, composites can be vulnerable to sudden impacts, which may cause invisible internal damage such as fiber breakage or delamination (Jones, 2013; Harris, 1999).

d. Challenges in Recycling:

Composites consist of different material phases that are hard to separate, which complicates recycling. This raises environmental concerns about long-term sustainability (Chawla, 2012; NATO Science Series, 2003).

e. Environmental Concerns:

The production of composites can be energy-intensive, and disposal options are limited due to poor recyclability. These environmental issues are a growing challenge, especially as their use becomes more widespread (Ashby, 2011; Yi & Zhang, 2006).

1.6. Conclusion

This chapter provided an overview of composite materials, covering their key components, types, and widespread applications in sectors like aerospace, automotive, and civil engineering. Composites have proven essential in meeting the demands of modern engineering due to their unique combination of strength, lightness, and durability. Moving forward, the future of composites will rely on advanced design processes that balance factors such as performance, cost, and sustainability, with design tools playing a crucial role in optimizing their use across various industries.

CHAPTER 2 :
PLATE THEORIES

2.1. Introduction

Laminated composite structures, composed of multiple bonded layers—often with distinct anisotropic properties—are widely used in engineering due to their excellent stiffness-to-weight and strength-to-weight ratios (Reddy, 2004; Jones, 1999). Given their small thickness relative to in-plane dimensions, they are typically modelled as plates for structural analysis.

To accurately predict their behavior under various loading conditions—including combined thermal and mechanical effects—numerous plate theories have been developed. These theories differ in their assumptions, mathematical complexity, and their ability to represent deformation through the thickness (Leissa, 1987; Reddy, 2004). While classical theories suffice for thin isotropic plates, more advanced formulations are necessary for thick or layered composites to account for shear deformation and interlaminar stresses (Carrera et al., 2011).

This chapter provides an overview of the principal plate theories used in the analysis of composite structures and sets the stage for the detailed derivations and comparisons that follow.

2.2. Material Behaviour in Composites

2.2.1. Generalised Hooke's Law For Composite Materials

In the study of composite materials, the generalized Hooke's law represents an extension of the classical formulation, adapted to the anisotropic and heterogeneous nature of such structures. Laminated composites, in particular, are assemblies of multiple homogeneous yet anisotropic layers, bonded together with varying fiber orientations. These structures typically possess a relatively small thickness compared to their other dimensions, making them highly suitable for numerous industrial and engineering applications (Jones, 1999; Reddy, 1997).

When describing the mechanical behavior of anisotropic materials, it becomes essential to express the relationship between stresses and strains using tensor notation. The stress tensor (σ_{ij}) and the strain tensor (ε_{ij}) are symmetric and can be represented in matrix form as:

$$(\sigma_{ij})=\begin{bmatrix}\sigma_{11} & \sigma_{12} & \sigma_{13}\\ \sigma_{21} & \sigma_{22} & \sigma_{23}\\ \sigma_{31} & \sigma_{32} & \sigma_{33}\end{bmatrix}, \tag{2.1}$$

$$(\varepsilon_{ij})=\begin{bmatrix}\varepsilon_{11} & \varepsilon_{12} & \varepsilon_{13}\\ \varepsilon_{21} & \varepsilon_{22} & \varepsilon_{23}\\ \varepsilon_{31} & \varepsilon_{32} & \varepsilon_{33}\end{bmatrix} \tag{2.2}$$

where:

- σ_{11} ,σ_{22} ,σ_{33} are normal stress components ,
- $\sigma_{12} = \sigma_{21}$,$\sigma_{13} = \sigma_{31}$,$\sigma_{23} = \sigma_{32}$ are the shear stress components ,
- ε_{11} , ε_{22} , ε_{33} are the normal strain components,
- $\varepsilon_{12} = \varepsilon_{21}$, $\varepsilon_{13} = \varepsilon_{31}$, $\varepsilon_{23} = \varepsilon_{32}$ are the shear strain components .

Due to the symmetry of the stress and strain tensors, the number of independent components is reduced to six. This reduction enables reformulation of the constitutive relationship into a compact matrix form. Thus, the generalized Hooke's law for composite materials can be expressed as:

$$\{\sigma\} = [C]\{\varepsilon\} \tag{2.3}$$

where:

- $\{\sigma\}$ is the 6 x 1 stress vector,
- $\{\varepsilon\}$ is the 6 x 1 strain vector,
- $[C]$ is the 6 x 6 stiffness matrix representing the elastic properties of the material (Reddy,1997).

The explicit form of the stiffness matrix $[C]$ is :

$$[c] = \begin{bmatrix} C_{11} & C_{12} & C_{13} & 0 & 0 & 0 \\ C_{21} & C_{22} & C_{23} & 0 & 0 & 0 \\ C_{31} & C_{32} & C_{33} & 0 & 0 & 0 \\ 0 & 0 & 0 & C_{44} & 0 & 0 \\ 0 & 0 & 0 & 0 & C_{55} & 0 \\ 0 & 0 & 0 & 0 & 0 & C_{66} \end{bmatrix} \tag{2.4}$$

Here, the terms C_{ij} represent the material stiffness coefficients. For orthotropic materials, the off-diagonal shear coupling terms are zero due to material symmetry (Jones, 1999). This matrix form facilitates the analysis of laminated composites by simplifying the directional dependency into a clear mathematical structure, essential for predicting their mechanical response under various loading conditions.

2.2.2. Different Types of Materials

The mechanical behavior of materials under loading is fundamentally influenced by their internal structure. In the context of composite materials and plate theories, it is essential to distinguish between different types of materials based on their mechanical symmetry and

response to external forces. The classification typically includes isotropic, anisotropic, orthotropic, and monoclinic materials (Gibson, 2016; Jones, 1999; Reddy, 1997).

a. Isotropic Materials

Isotropic materials possess identical mechanical properties in all directions. Their behavior is independent of the orientation of the applied load. The elastic constants, such as Young's modulus *E,* Poisson's ratio ν, and shear modulus *G*, are uniform throughout the material.

For isotropic materials, the stiffness matrix $[C]$ simplifies significantly and can be expressed in terms of two independent elastic constants, C_{11} and C_{12}. The constitutive relationship is:

$$[C]=\begin{bmatrix} C_{11} & C_{12} & C_{12} & 0 & 0 & 0 \\ C_{12} & C_{11} & C_{12} & 0 & 0 & 0 \\ C_{12} & C_{12} & C_{11} & 0 & 0 & 0 \\ 0 & 0 & 0 & C_{44} & 0 & 0 \\ 0 & 0 & 0 & 0 & C_{44} & 0 \\ 0 & 0 & 0 & 0 & 0 & C_{44} \end{bmatrix} \tag{2.5}$$

where :

$$C_{11}=\frac{E(1-\nu)}{(1+\nu)(1-2\nu)} \quad , C_{12}=\frac{E\nu}{(1+\nu)(1-2\nu)} \quad , C_{44}=\frac{E\nu}{2(1+\nu)} \tag{2.6}$$

Thus, only two independent constants E and υ (or equivalently, C_{11} and C_{12} are needed to describe an isotropic material (Jones, 1999). Examples of isotropic materials include metals like steel and aluminum, and many ceramics.

b. Anisotropic Materials

Anisotropic materials exhibit different mechanical properties in different directions. Their stiffness, strength, and deformation behavior vary depending on the loading orientation. In the most general case, the stiffness matrix [C] for a fully anisotropic material contains 21 independent constants and is symmetric:

$$[C]=\begin{bmatrix} C_{11} & C_{12} & C_{13} & C_{14} & C_{15} & C_{16} \\ & C_{22} & C_{23} & C_{24} & C_{25} & C_{26} \\ & & C_{33} & C_{34} & C_{35} & C_{36} \\ & & & C_{44} & C_{45} & C_{46} \\ & & & & C_{55} & C_{56} \\ & & & & & C_{66} \end{bmatrix} \quad (2.7)$$

Symmetry implies that $C_{ij} = C_{ji}$ (Reddy, 1997). Fully anisotropic materials, such as certain crystals and complex composite laminates, require a complete set of 21 independent elastic constants for their description.

c. Orthotropic Materials

Orthotropic materials are a specialized form of anisotropic materials with three mutually perpendicular planes of symmetry. Their mechanical properties differ along three principal material axes but remain constant within each principal plane.

The stiffness matrix $[C]$for an orthotropic material simplifies to:

$$[c]=\begin{bmatrix} C_{11} & C_{12} & C_{13} & 0 & 0 & 0 \\ C_{21} & C_{22} & C_{23} & 0 & 0 & 0 \\ C_{31} & C_{32} & C_{33} & 0 & 0 & 0 \\ 0 & 0 & 0 & C_{44} & 0 & 0 \\ 0 & 0 & 0 & 0 & C_{55} & 0 \\ 0 & 0 & 0 & 0 & 0 & C_{66} \end{bmatrix} \quad (2.4)$$

Only nine independent constants are required to describe an orthotropic material (Gibson, 2016). Typical examples include laminated fiber-reinforced composites, wood, and rolled metal sheets.

d. Monoclinic Materials

Monoclinic materials exhibit a single plane of material symmetry, making their behavior less symmetric than orthotropic materials but more structured than fully anisotropic ones. They require 13 independent elastic constants when the symmetry plane is taken as the 1-2 plane (X-Y plane).

The stiffness matrix $[C]$ for monoclinic materials is:

$$[C]=\begin{bmatrix} C_{11} & C_{12} & C_{13} & 0 & C_{15} & 0 \\ C_{12} & C_{22} & C_{23} & 0 & C_{25} & 0 \\ C_{13} & C_{23} & C_{33} & C_{34} & C_{35} & 0 \\ 0 & 0 & 0 & C_{44} & 0 & C_{46} \\ C_{15} & C_{25} & C_{35} & 0 & C_{55} & 0 \\ 0 & 0 & 0 & C_{46} & 0 & C_{66} \end{bmatrix} \tag{2.8}$$

Examples include certain polymer composites and geological materials like shale (Reddy, 1997).

2.2.3. Ply-Level Stress-Strain and Displacement Relationships

In composite laminates, each individual ply can be modeled as an anisotropic or orthotropic material. The mechanical behavior of a single ply is described first in its own material coordinate system, and then transformed if the ply is oriented at an angle relative to the laminate axes.

a. Reduced Stiffness Matrix $[\boldsymbol{Q}]$

In the local material axes (fiber directions, denoted 1–2), the constitutive relationship for an individual ply is:

$$\begin{bmatrix} \sigma_1 \\ \sigma_2 \\ \tau_{12} \end{bmatrix}=\begin{bmatrix} Q_{11} & Q_{12} & 0 \\ Q_{12} & Q_{22} & 0 \\ 0 & 0 & Q_{66} \end{bmatrix}\begin{bmatrix} \varepsilon_1 \\ \varepsilon_2 \\ \gamma_{12} \end{bmatrix} \tag{2.9}$$

where :

- σ_1, σ_2 are the normal stresses ,
- τ_{12} is the in-plane shear stress ,
- $\varepsilon_1, \varepsilon_2$ are the normal strains ,
- γ_{12} is the engineering shear strain.

The reduced stiffness components are:

$$Q_{11}=\frac{E_1}{1-\nu_{12}\nu_{21}}, \qquad Q_{22}=\frac{E_2}{1-\nu_{12}\nu_{21}}, \qquad Q_{12}=\frac{\nu_{12}E_2}{1-\nu_{12}\nu_{21}}, \qquad Q_{66}=G_{12} \tag{2.10}$$

where :

- E_1, E_2 are Young's moduli along and transverse to the fiber ,

- G_{12} is the in-plane shear modulus ,
- ν_{12} is the major Poisson's ratio (Daniel & Ishai, 2006; Jones, 1999).

b. Transformed Reduced Stiffness Matrix $[\bar{Q}]$

If a ply is oriented at an angle θ with respect to the laminate axes (global x-y coordinates), its stiffness must be transformed. The transformed reduced stiffness matrix is:

$$\left[\bar{Q}\right] = \begin{bmatrix} \overline{Q_{11}} & \overline{Q_{12}} & \overline{Q_{16}} \\ \overline{Q_{12}} & \overline{Q_{22}} & \overline{Q_{26}} \\ \overline{Q_{16}} & \overline{Q_{26}} & \overline{Q_{66}} \end{bmatrix} \tag{2.11}$$

$$\begin{Bmatrix} \sigma_x \\ \sigma_y \\ \tau_{xy} \end{Bmatrix} = \begin{bmatrix} \bar{Q}_{11} & \bar{Q}_{12} & \bar{Q}_{16} \\ \bar{Q}_{12} & \bar{Q}_{22} & \bar{Q}_{26} \\ \bar{Q}_{16} & \bar{Q}_{26} & \bar{Q}_{66} \end{bmatrix} \begin{Bmatrix} \varepsilon_x \\ \varepsilon_y \\ \gamma_{xy} \end{Bmatrix} \tag{2.12}$$

with components :

$$\begin{aligned}
\overline{Q_{11}} &= Q_{11}\cos^4\theta + 2(Q_{12}+2Q_{66})\sin^2\theta\cos^2\theta + Q_{22}\sin^4\theta \\
\overline{Q_{22}} &= Q_{11}\sin^4\theta + 2(Q_{12}+2Q_{66})\sin^2\theta\cos^2\theta + Q_{22}\cos^4\theta \\
\overline{Q_{12}} &= (Q_{11}+Q_{22}+4Q_{66})\sin^2\theta\cos^2\theta + Q_{12}(\sin^4\theta+\cos^4\theta) \\
\overline{Q_{66}} &= (Q_{11}+Q_{22}-2Q_{12}-2Q_{66})\sin^2\theta\cos^2\theta + Q_{66}(\sin^4\theta+\cos^4\theta) \\
\overline{Q_{16}} &= (Q_{11}-Q_{12}-2Q_{66})\cos^3\theta\sin\theta - (Q_{22}-Q_{12}-2Q_{66})\sin^3\theta\cos\theta \\
\overline{Q_{26}} &= (Q_{11}-Q_{12}-2Q_{66})\sin^3\theta\cos\theta - (Q_{22}-Q_{12}-2Q_{66})\cos^3\theta\sin\theta
\end{aligned} \tag{2.13}$$

(Jones, 1999; Kaw,2006)

The transformed matrix $[\bar{Q}]$ allows each ply, regardless of fiber orientation, to contribute correctly to the overall laminate stiffness.

2.2.4. Laminate-Level Constitutive Equations

Once the transformed properties of individual plies are known, the overall mechanical behaviour of the laminate can be established.

a. Stress and Moment Resultants

The laminate behaviour is summarized by defining in-plane force resultants and bending moment resultants.

i. In-plane force resultants

$$N_x = \int_{-h/2}^{h/2} \sigma_x(z)dz$$

$$N_y = \int_{-h/2}^{h/2} \sigma_y(z)dz \qquad (2.14)$$

$$N_{xy} = \int_{-h/2}^{h/2} \tau_{xy}(z)dz$$

ii. Bending Moment Resultants

$$M_x = \int_{-h/2}^{h/2} \sigma_x(z)zdz$$

$$M_y = \int_{-h/2}^{h/2} \sigma_y(z)zdz \qquad (2.15)$$

$$M_{xy} = \int_{-h/2}^{h/2} \tau_{xy}(z)zdz$$

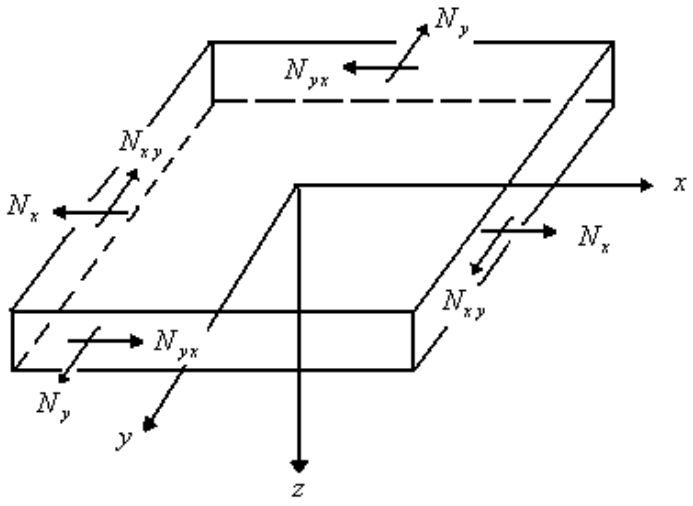

Figure 17:Membrane Force Resultants

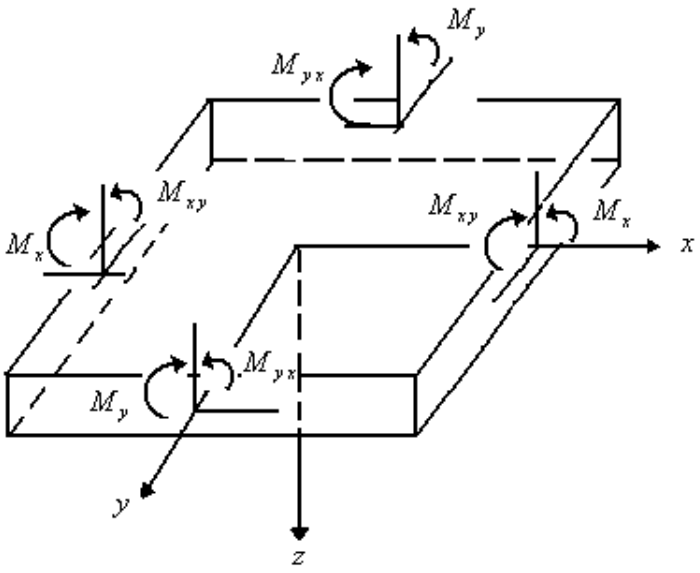

Figure 18:Membrane bending moment resultants

where z is the distance from the mid-plane, and h is the total laminate thickness (Reddy, 1997).

b. Laminate Constitutive Equation (ABD Matrices)

The laminate-level constitutive relation is:

$$\begin{bmatrix} N_x \\ N_y \\ N_{xy} \\ M_x \\ M_y \\ M_{xy} \end{bmatrix} = \begin{bmatrix} A_{11} & A_{12} & A_{16} & B_{11} & B_{12} & B_{16} \\ A_{12} & A_{22} & A_{26} & B_{12} & B_{22} & B_{26} \\ A_{16} & A_{26} & A_{66} & B_{16} & B_{26} & B_{66} \\ B_{11} & B_{12} & B_{16} & D_{11} & D_{12} & D_{16} \\ B_{12} & B_{22} & B_{26} & D_{12} & D_{22} & D_{26} \\ B_{16} & B_{26} & B_{66} & D_{16} & D_{26} & D_{66} \end{bmatrix} \begin{bmatrix} \varepsilon_{xx}^0 \\ \varepsilon_{yy}^0 \\ \gamma_{xy}^0 \\ \kappa_x \\ \kappa_y \\ \kappa_{xy} \end{bmatrix} \tag{2.16}$$

Where :

- ε_{xx}^0 , ε_{yy}^0 , γ_{xy}^0 are mid-plane strains ,
- κ_x , κ_y , κ_{xy} are mid-plane curvatures ,
- $[\boldsymbol{A}]$ is the extensional stiffness matrix ,
- $[\boldsymbol{B}]$ is the bending-stretching coupling matrix ,
- $[\boldsymbol{D}]$ is the bending stiffness matrix .

c. Construction of [A], [B], and [D] Matrices

The elements of the stiffness matrices are constructed by summing contributions from each ply:

$$A_{ij} = \sum_{k=1}^{n} \overline{Q_{ij}^{(k)}} (z_k - z_{k-1}) \tag{2.17}$$

$$B_{ij} = \frac{1}{2} \sum_{k=1}^{n} \overline{Q_{ij}^{(k)}} (z_k^2 - z_{k-1}^2) \tag{2.18}$$

$$D_{ij} = \frac{1}{3} \sum_{k=1}^{n} \overline{Q_{ij}^{(k)}} (z_k^3 - z_{k-1}^3) \tag{2.19}$$

Where :

- z_k and z_{k-1} are the vertical coordinates of the top and bottom surfaces of the *k*-th ply and
- n is the total number of plies (Daniel & Ishai, 2006).

For symmetric laminates, the bending-stretching coupling matrix B vanishes, i.e., B=0, resulting in uncoupled behaviour where in-plane loads produce only mid-plane strains, and bending moments produce only curvatures (Jones, 1999; Kaw, 2006).

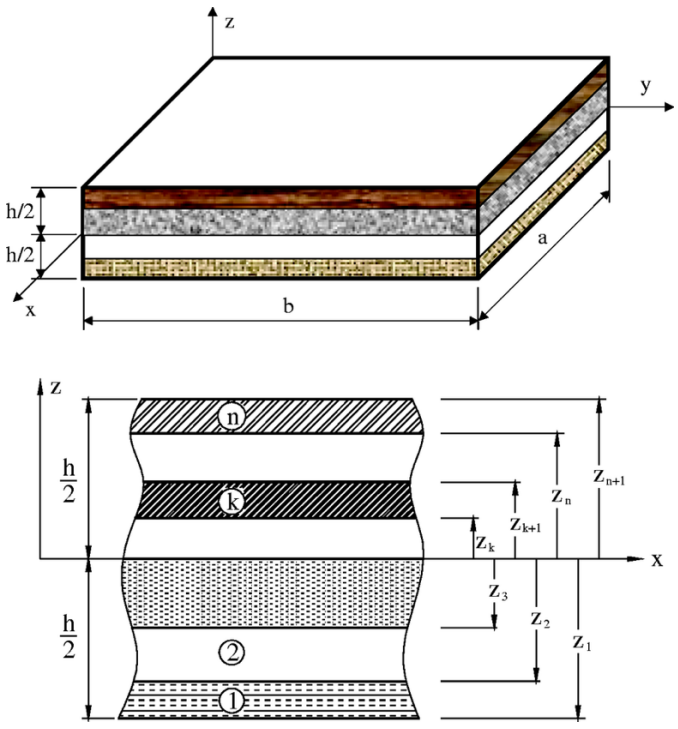

Figure 19:Layer-numbering used for a typical laminate

2.2.5. Displacement Fields and Deformation Fields

In the analysis of laminated composite plates, the displacement field describes the movement of a material point from its initial position under mechanical or thermal loading. For a point located at (x, y, z) within the plate, the displacement vector is expressed as:

$$u(x,y,z) = \begin{bmatrix} u(x,y,z) \\ v(x,y,z) \\ w(x.y,z) \end{bmatrix} \tag{2.20}$$

Where u , v ,and w are the displacements in the longitudinal (x), transverse (y) , and thickness (z) directions , respectively (Reddy,2004 ; Jones,1999).

To simplify this representation, the displacement field is typically defined relative to the mid-plane of the plate, located at $z = 0$. This allows the decomposition of displacements into mid-plane displacements and their variation through the thickness:

$$\begin{aligned} u(x,y,z) &= u_0(x,y) + z\phi_x(x,y) \\ v(x,y,z) &= v_0(x,y) + z\phi_y(x,y) \\ w(x,y,z) &= w_0(x,y) \end{aligned} \tag{2.21}$$

Where:

- $u_0(x,y)$, $v_0(x,y)$: in-plane displacements of the mid-surface,
- $w_0(x,y)$: transverse deflection of the mid-surface,
- $\emptyset_x(x,y)$, $\emptyset_y(x,y)$: rotational functions representing the slope of the transverse displacement w_0 about the y- and x- axes respectively (Carrera et al.; Noor & Burton,1990).

These functions account for the rotation of normals to the mid-surface and are essential for capturing bending and transverse shear effects, particularly in thick or multilayered plates.

From these displacement expressions, the strain components (deformation field) can be derived using the linear strain-displacement relations:

$$\varepsilon_{xx} = \frac{\partial u}{\partial x} = \frac{\partial u_0}{\partial x} + z\frac{\partial \phi_x}{\partial x} \tag{2.22}$$

$$\varepsilon_{yy} = \frac{\partial v}{\partial y} = \frac{\partial v_0}{\partial y} + z\frac{\partial \phi_y}{\partial y} \tag{2.23}$$

$$\gamma_{xy} = \frac{\partial u}{\partial y} + \frac{\partial v}{\partial x} = \frac{\partial u_0}{\partial y} + \frac{\partial v_0}{\partial x} + z\left(\frac{\partial \phi_x}{\partial y} + \frac{\partial \phi_y}{\partial x}\right) \tag{2.24}$$

$$\gamma_{xz} = \frac{\partial u}{\partial z} + \frac{\partial w}{\partial x} = \phi_x + \frac{\partial w_0}{\partial x} \tag{2.25}$$

$$\gamma_{yz} = \frac{\partial v}{\partial z} + \frac{\partial w}{\partial y} = \phi_y + \frac{\partial w_0}{\partial y} \tag{2.26}$$

These relations demonstrate how both mid-plane strains and curvatures contribute to the total deformation. The transverse shear strains γ_{xz} and γ_{yz} include contributions from both the slopes of the transverse displacement and the rotation functions ,which are relevant in shear-deformable theories (Reddy,2004).

2.3. Plate Theories

The structural analysis of laminated composite plates requires simplifications of the full three-dimensional elasticity theory due to the complexity introduced by their layered and anisotropic nature. To address this, various plate theories have been developed that approximate the plate's behavior using two-dimensional models based on suitable kinematic assumptions (Reddy, 2004; Carrera, 2002).

These theories are generally classified into the following three groups:

- Equivalent Single Layer (ESL) models
- Layerwise models
- Asymptotic and multiscale methods

2.3.1. Equivalent Single Layer Models

Equivalent Single Layer (ESL) models represent the entire laminate as a single homogenized plate with a unified displacement field across the thickness. They are efficient for thin to moderately thick composite plates and are commonly used in structural analysis (Reddy, 2004).

The main ESL theories include:

- Classical Plate Theory (CPT)
- First-Order Shear Deformation Theory (FSDT)
- Higher-Order Shear Deformation Theories (HSDT)

a. Classical Plate Theory (CPT)

The Classical Plate Theory (CPT), also known as the Kirchhoff-Love plate theory, is the foundational model in the analysis of thin plates. It assumes that the plate's thickness is small compared to its in-plane dimensions, and it neglects transverse shear deformation. This makes the theory suitable for slender, thin laminates but less accurate for moderately thick or thick plates (Reddy, 2004; Leissa, 1969).

CPT is based on the following key assumptions:

1. The plate is thin , its thickness is much smaller compared to its in-plane dimensions.
2. Normals to the mid-surface remain straight and normal after deformation (no transverse shear deformation).
3. Normals do not change in length (no thickness stretch).
4. Displacements and strains are small.
5. The material is linearly elastic and follows Hooke's law.

i. Displacement Field

In CPT, the displacement field at any point (x, y, z) in the plate is expressed in terms of the mid-plane displacements:

$$\begin{aligned} u(x,y,z) &= u_0(x,y) - z\frac{\partial w_0}{\partial x} \\ v(x,y,z) &= v_0(x,y) - z\frac{\partial w_0}{\partial y} \\ w(x,y,z) &= w_0(x,y) \end{aligned} \tag{2.27}$$

Where:

- $u_0(x,y)$ and $v_0(x,y)$ are the in-plane displacements at the mid-plane,
- $w_0(x,y)$ represents the transverse displacement (out-of-plane),
- z denotes the distance from the mid-surface (positive in the upward direction).

This field reflects the assumption that normals rotate due to bending but do not experience shear or stretch (Timoshenko & Woinowsky-Krieger, 1959).

ii. Strain-Displacement Relations

Based on linear elasticity and small deformations, the in-plane strain components are:

$$\varepsilon_{xx} = \frac{\partial u}{\partial x} = \frac{\partial u_0}{\partial x} - z\frac{\partial^2 w_0}{\partial x^2} \tag{2.28}$$

$$\varepsilon_{yy} = \frac{\partial v}{\partial y} = \frac{\partial v_0}{\partial y} - z\frac{\partial^2 w_0}{\partial y^2} \tag{2.29}$$

$$\gamma_{xy} = \frac{\partial u}{\partial y} + \frac{\partial v}{\partial x} = \frac{\partial u_0}{\partial y} + \frac{\partial v_0}{\partial x} - 2z\frac{\partial^2 w_0}{\partial x \partial y} \tag{2.30}$$

No transverse shear strains (γ_{xz}, γ_{yz}) appear in CPT because of the assumption of inextensible normals (Love, 1944).

Although CPT is widely used for its simplicity and analytical tractability ,it has several limitations :

- It ignores transverse shear deformation, making it unsuitable for thick plates.
- It cannot capture interlaminar stresses, which are crucial in composite laminates.
- It underestimates deflections and overestimates stiffness in moderately thick plates (Noor & Burton, 1990).

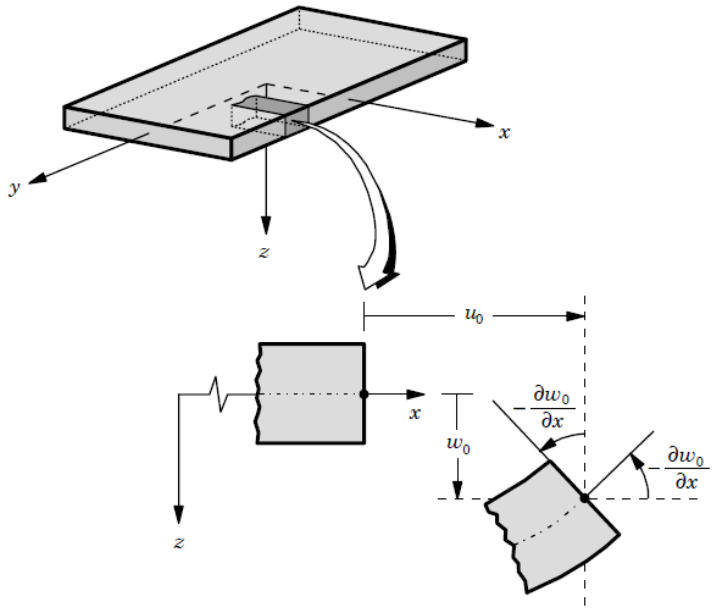

Figure 20:Kinematics of the Love Kirchhoff (Reddy, 1997) - CPT.

b. First-Order Shear Deformation Theory (FSDT)

The First-Order Shear Deformation Theory (FSDT), also known as Mindlin-Reissner theory, was developed to improve upon the Classical Plate Theory (CPT) by incorporating transverse shear deformation. Unlike CPT, which is suitable only for very thin plates, FSDT can accurately

model the behavior of moderately thick plates where shear effects are non-negligible (Mindlin, 1951; Reddy, 2004).

FSDT is based on the main key assumptions :

1. The plate is moderately thick ; transverse shear deformation is considered.
2. Normals to the mid-surface before deformation remain straight but not necessarily perpendicular to the mid-surface after deformation.
3. Normals do not stretch (no thickness deformation).
4. Transverse shear strains are constant through the thickness.
5. A shear correction factor is introduced to compensate for the constant shear strain assumption.
6. Material behaviour is linear elastic, and displacements are small

i. Displacement Field

The displacement components *u(x,y,z), v(x,y,z), w(x,y,z)* at any point in the plate are expressed as:

$$\begin{aligned} u(x,y,z) &= u_0(x,y) + z\phi_x(x,y) \\ v(x,y,z) &= v_0(x,y) + z\phi_y(x,y) \\ w(x,y,z) &= w_0(x,y) \end{aligned} \tag{2.31}$$

Where:

- $u_0(x,y)$, $v_0(x,y)$: in-plane displacements of the mid-surface,
- $w_0(x,y)$: transverse displacement of the mid-surface,
- $\emptyset_x(x,y)$, $\emptyset_y(x,y)$: rotations of the normal to the mid-surface about the *y*- and *x*- axes respectively.

This formulation allows for transverse shear deformation, improving accuracy for thicker plates (Reissner, 1945; Reddy, 2004).

ii. Strain-Displacement Relations

The in-plane and shear strains are given as:

$$\varepsilon_{xx} = \frac{\partial u}{\partial x} = \frac{\partial u_0}{\partial x} + z\frac{\partial \phi_x}{\partial x} \tag{2.32}$$

$$\varepsilon_{yy} = \frac{\partial v}{\partial y} = \frac{\partial v_0}{\partial y} + z\frac{\partial \phi_y}{\partial y} \tag{2.33}$$

$$\gamma_{xy} = \frac{\partial u}{\partial y} + \frac{\partial v}{\partial x} = \frac{\partial u_0}{\partial y} + \frac{\partial v_0}{\partial x} + z\left(\frac{\partial \phi_x}{\partial y} + \frac{\partial \phi_y}{\partial x}\right) \tag{2.34}$$

$$\gamma_{xz} = \frac{\partial u}{\partial z} + \frac{\partial w}{\partial x} = \phi_x + \frac{\partial w_0}{\partial x} \tag{2.35}$$

$$\gamma_{yz} = \frac{\partial v}{\partial z} + \frac{\partial w}{\partial y} = \phi_y + \frac{\partial w_0}{\partial y} \tag{2.36}$$

Unlike CPT, transverse shear strains γ_{xz} , γ_{yz} are not zero ,enabling FSDT to capture shear effects with improved accuracy, particularly for moderately thick plates. However ,FSDT presents several limitations:

1. It assumes transverse shear strains are constant through the thickness.
2. It requires shear correction factors.
3. Suitable for moderately thick plates ;tends to lose accuracy when applied to thick plates.

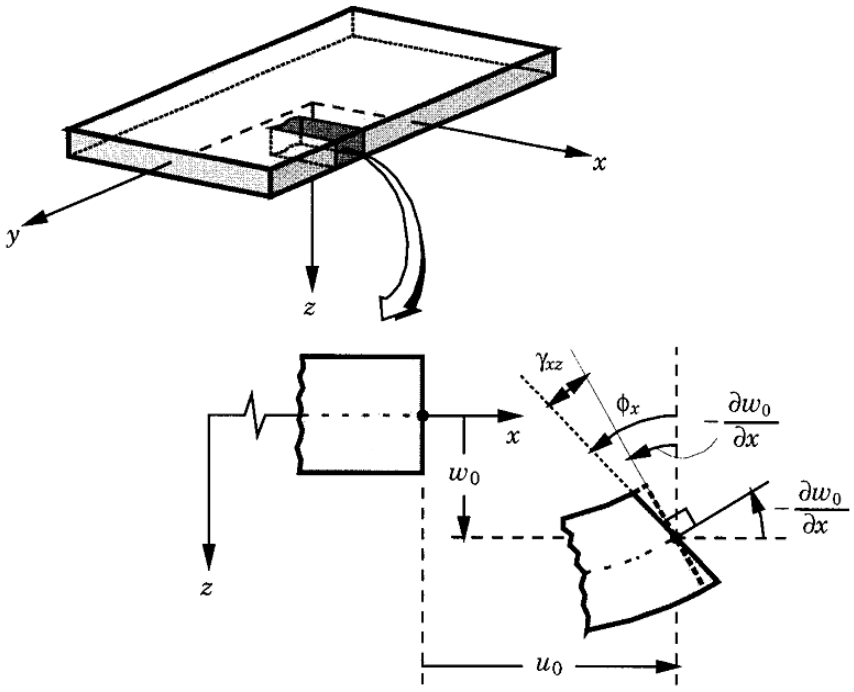

Figure 21:Kinematics of Reissner-Mindlin.

c. High-Order Shear Deformation Theory (HSDT)

To overcome the limitations of the Classical Plate Theory (CPT) and First-Order Shear Deformation Theory (FSDT), the Higher-Order Shear Deformation Theory (HSDT) introduces a more refined representation of the displacement field by allowing nonlinear variation of transverse shear strains through the plate's thickness. This approach satisfies zero shear stress conditions at the plate surfaces, thus eliminating the need for shear correction factors (Reddy, 1984; Carrera, 2003).

Key features of this theory are :

1. Transverse shear deformation is modelled using a higher-order variation that satisfies shear stress-free boundary conditions at the top and bottom surfaces.
2. Small deformations and linear elastic behavior are assumed.
3. Suitable for thick and moderately thick composite laminates and sandwich structures.

i. Displacement Field Using a Generalized Shape Function

The displacement components are defined as:

$$\begin{aligned} u(x,y,z) &= u_0(x,y) + z\phi_x(x,y) + f(z)\theta_x(x,y) \\ v(x,y,z) &= v_0(x,y) + z\phi_y(x,y) + f(z)\theta_y(x,y) \\ w(x,y,z) &= w_0(x,y) \end{aligned} \tag{2.37}$$

Where :

- u_0 , v_0 , w_0 are mid-plane displacements,
- $\emptyset_x(x,y)$, $\emptyset_y(x,y)$ are the rotations due to bending,
- θ_x , θ_y are higher-order shear rotations,
- *f(z)* is a shear strain function satisfying $f(\pm {}^{h}/_{2}) = 0$.

Several forms of *f(z)* have been proposed in the literature to ensure accurate shear strain distribution and satisfy boundary conditions:

- Reddy's Third-Order Polynomial (Reddy,1984):

$$f(z) = z - \frac{4z^3}{3h^2} \tag{2.38}$$

- Carrera Unified Formulation (CUF) (Carrera, 2003):

$$f(z) = z^3 - \frac{3zh^2}{4} \tag{2.39}$$

- Touratier's Trigonometric Function (Touratier, 1991):

$$f(z) = \sin(\frac{\pi z}{h}) \tag{2.40}$$

Each of these functions can be tailored for specific applications, with trigonometric and exponential forms offering better performance for certain geometries and boundary conditions.

ii. Strain-Displacement Relations

The transverse shear strains are derived from the displacement field:

$$\gamma_{xz} = \frac{\partial w_0}{\partial x} + \phi_x + f'(z)\theta_x \tag{2.41}$$

$$\gamma_{yz} = \frac{\partial w_0}{\partial y} + \phi_y + f'(z)\theta_y \tag{2.42}$$

Where *f'(z)* is the derivative of the shape function with respect to z .

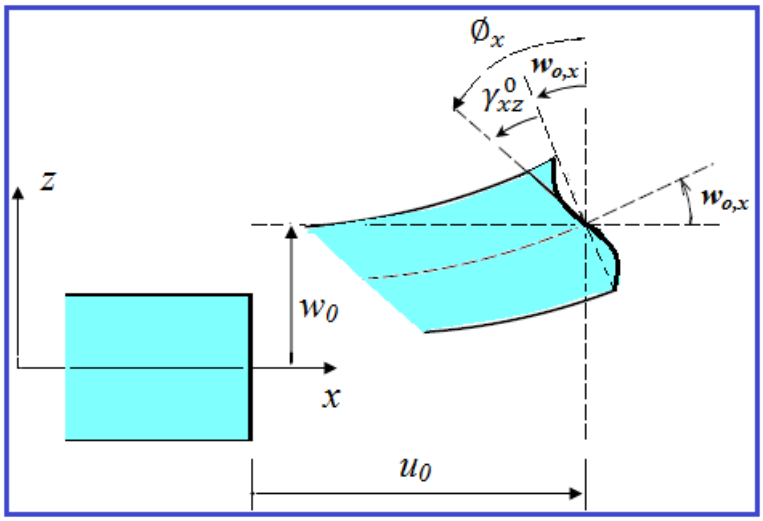

Figure 22:Kinematics of HSDT

2.3.2. Layerwise Models

Layerwise models represent advanced theories in the analysis of laminated composite plates. Unlike Equivalent Single Layer (ESL) models, which assume homogenized properties through

the thickness, layerwise approaches account for the distinct mechanical behavior of each layer. This enables a more accurate prediction of interlaminar stresses and deformations, especially in applications involving thick laminates, heterogeneous stacking sequences, and delamination phenomena (Reddy, 2004; Carrera, 2003).

a. Zig-Zag Models

Zig-zag models are a class of layerwise theories that allow for discontinuities in the slope of the in-plane displacement fields across layer interfaces. These slope jumps result in a zig-zag pattern in the deformation field, enabling the model to represent shear discontinuities between adjacent layers (Murakami, 1986; Di Sciuva, 1986). This is particularly beneficial for laminated composites where significant contrasts in mechanical properties exist between layers. Zig-zag models provide improved accuracy over classical and first-order shear deformation theories, especially for laminated structures with marked differences in stiffness between plies. They offer a good balance between computational efficiency and the ability to represent interlaminar behavior more realistically.

b. Discrete Layer Models

Discrete layer models treat each ply in the laminate as an independent mechanical entity with its own displacement variables. Unlike zig-zag models, which approximate interfacial behavior, discrete layer models fully resolve the displacement and stress fields in each layer through individual finite element formulations (Tessler & Di Sciuva, 1993; Carrera & Petrolo, 2011). This results in high-fidelity representation of layerwise interactions and interlaminar stress distributions, making these models especially suitable for detailed analyses of sandwich structures, delamination, and damage initiation.

Both zig-zag and discrete layer models represent significant advances over ESL theories. While zig-zag models maintain a lower computational cost and sufficient accuracy for many engineering applications, discrete layer models are preferred for high-precision simulations where through-thickness stress resolution is critical.

2.3.3. Asymptotic and Multiscale Methods

Asymptotic and multiscale methods are advanced approaches used to improve plate theories by starting from the full three-dimensional elasticity equations. These methods are especially useful for composite plates, where the material properties change from one layer to another. Asymptotic methods take advantage of the fact that plates are usually thin compared to their

other dimensions. Using this thickness-to-length ratio as a small parameter, the solution is written as a series expansion (Sanchez-Palencia, 1980; Berdichevsky, 1990). The method separates the overall (global) behavior from local effects near the edges, where stress changes are more significant. These local effects, known as boundary layers, are added as corrections to improve accuracy (Ladeveze, 1988; Allix, 1989).

Multiscale methods aim to link the small-scale behavior of materials (like the fibers and matrix in composites) to the overall behavior of the plate. They do this by solving problems at two levels: the macroscale (the whole plate) and the microscale (each layer or material component). This helps predict the stiffness and stresses more accurately, especially in materials with complex internal structures (Fish & Yu, 2001; Miehe & Koch, 2002).

These methods allow for better modeling of composite plates by capturing both detailed local behavior and overall structural response, without needing to fully solve a complex 3D model.

2.4. Conclusion

This chapter presented various plate theories for analyzing composite structures, ranging from classical models to more advanced approaches. While classical theories are suitable for thin plates with simple material behavior, more refined models—such as layerwise and multiscale methods—are necessary for accurately modeling thick, multilayered, and heterogeneous composites. The choice of theory depends on factors such as plate thickness, material complexity, and the required level of accuracy in capturing interlaminar stresses and deformation.

Chapter 3 :

MATHEMATICAL FORMULATIONS

3.1. Introduction

Rectangular laminated plates are widely used in structural applications where thermal loads act. Accurate static analysis under such loading is essential for safe and efficient design.

This chapter presents the mathematical formulation for the static analysis of simply supported cross-ply laminated plates using a refined displacement field. The proposed model aims to improve the accuracy of displacement and stress predictions under thermal loading.

3.2. Geometrical Configuration

Consider a rectangular cross-ply laminated composite plate subjected to thermal loading. The plate has length ,width ,and thickness denoted by a ,b ,and h ,respectively. A global Cartesian coordinate system (*x,y,z*) is adopted , with the origin located at the corner and on the mid-plane of the plate (z=0). Accordingly ,the geometric domain of the plate is defined as:

$$0 \leq x \leq a \ ;$$

$$0 \leq y \leq b \ ;4$$

$$\frac{-h}{2} \leq z \leq \frac{h}{2}.$$

In this configuration:

- *x* and *y* represent the in-plane dimensions of the plate.
- *z* denotes the thickness direction , with *z*=0 on the mid-surface. The thickness extends from –h/2 to h/2 .

This geometrical configuration provides an effective basis for modelling the static behavior of the laminated plate under thermal loads using the proposed displacement field.

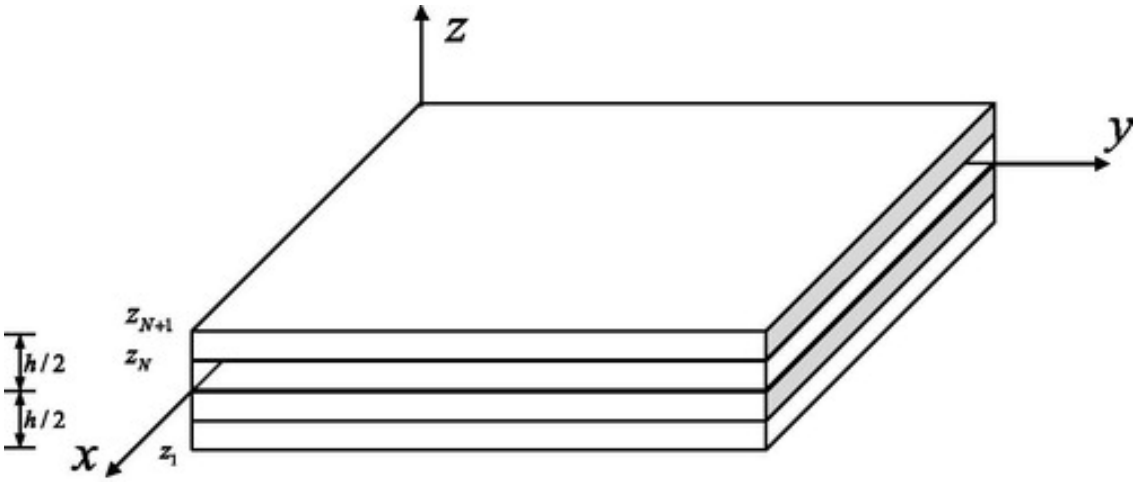

Figure 23:Coordinate system of the laminated plate

3.3. Displacement Field

Based on the higher order shear deformation theory, a refined displacement field (Mantari et al, 2012) is employed in this study. This formulation depends on the use of a parameter "m" , whose values were determined so as to give results closets to the 3D elasticity bending solution. It is designed to enhance the accuracy of the static analysis of cross-ply laminated composite plates subjected to thermal loading. The displacement components in the x, y, and z directions are defined as follows:

$$u(x,y,z) = u_0(x,y) + z[-m\sec^2(m\frac{h}{2})\theta_1 - \frac{\partial w_0}{\partial x}] + \tan mz\theta_1$$

$$\mathrm{v}(x,y,z) = v_0(x,y) + z[-m\sec^2(m\frac{h}{2})\theta_2 - \frac{\partial w_0}{\partial y}] + \tan mz\theta_2 \qquad (3.1)$$

$$\mathrm{w}(x,y,z) = w_0(x,y)$$

Assuming that $y^* = -m\sec^2(\alpha)$, $\psi(z) = \tan mz$, $f(z) = \tan mz + y^* z$, and $\alpha = m\frac{h}{2}$,the displacement field of this study can be rewritten as :

$$u(x,y,z) = u_0(x,y) + z[y^*\theta_{1(x,y)} - \frac{\partial w_0}{\partial x}(x,y)] + \psi(z)\theta_{1(x,y)}$$

$$\mathrm{v}(x,y,z) = v_0(x,y) + z[y^*\theta_{2(x,y)} - \frac{\partial w_0}{\partial y}(x,y)] + \psi(z)\theta_{2(x,y)} \qquad (3.2)$$

$$\mathrm{w}(x,y,z) = w_0(x,y)$$

With:

- u ,v ,w as the displacements along the x ,y ,z directions ,respectively
- u_0 , v_0 , w_0, θ_1, θ_2 are the five unknown functions of the middle surface of the plate
- $f(z)$ representing the shape function determining the distribution of the transverse shear strains and stresses along the thickness.

3.4. Deformation Field

The linear strain expressions derived from the displacement field are as follows:

$$\varepsilon_{xx} = \frac{\partial u}{\partial x} = \frac{\partial u_0}{\partial x} + zy^* \frac{\partial \theta_1}{\partial x} - z\frac{\partial^2 w_0}{\partial x^2} + \psi(z)\frac{\partial \theta_1}{\partial x}$$

$$\varepsilon_{yy} = \frac{\partial v}{\partial y} = \frac{\partial v_0}{\partial y} + zy^* \frac{\partial \theta_2}{\partial y} - z\frac{\partial^2 w_0}{\partial y^2} + \psi(z)\frac{\partial \theta_2}{\partial y}$$

$$\gamma_{xy} = \frac{\partial u}{\partial y} + \frac{\partial v}{\partial x} = \frac{\partial u_0}{\partial y} + \frac{\partial v_0}{\partial x} + zy^* \frac{\partial \theta_1}{\partial y} + zy^* \frac{\partial \theta_2}{\partial x} - 2z\frac{\partial^2 w_0}{\partial x \partial y} + \psi(z)[\frac{\partial \theta_1}{\partial y} + \frac{\partial \theta_2}{\partial x}] \quad (3.3)$$

$$\gamma_{yz} = \frac{\partial v}{\partial z} + \frac{\partial w}{\partial y} = y^* \theta_{2(x,y)} + \frac{\partial \psi(z)}{\partial z}\theta_{2(x,y)}$$

$$\gamma_{xz} = \frac{\partial u}{\partial z} + \frac{\partial w}{\partial x} = y^* \theta_{1(x,y)} + \frac{\partial \psi(z)}{\partial z}\theta_{1(x,y)}$$

With: $m\sec^2 mz = \frac{\partial \psi(z)}{\partial z} = g(\mathrm{z})$

3.5. Stress Field

The stress field is given by Hooke's Law as follows:

$$\begin{Bmatrix} \sigma_{xx} \\ \sigma_{yy} \\ \tau_{xy} \end{Bmatrix}_{(k)} = \begin{bmatrix} Q_{11} & Q_{12} & 0 \\ Q_{12} & Q_{22} & 0 \\ 0 & 0 & Q_{66} \end{bmatrix}_{(\mathrm{k})} \begin{Bmatrix} \varepsilon_{xx} - \alpha_1 T \\ \varepsilon_{yy} - \alpha_2 T \\ \gamma_{xy} \end{Bmatrix}_{(k)} \quad (3.4)$$

$$\begin{Bmatrix} \tau_{yz} \\ \tau_{xz} \end{Bmatrix}_{(k)} = \begin{bmatrix} Q_{44} & 0 \\ 0 & Q_{55} \end{bmatrix}_{(\mathrm{k})} \begin{Bmatrix} \gamma_{yz} \\ \gamma_{xz} \end{Bmatrix}_{(k)}$$

Where (σ_{xx} , σ_{yy} τ_{xy} , τ_{yz} τ_{xz}) and (ε_{xx} , ε_{yy} , γ_{xy} γ_{yz} γ_{xz}) are the components of stress and strain ,respectively .The stiffness coefficients Q_{ij} can be expressed in terms of engineering constants as follows :

$$Q_{11} = \frac{E_1}{1-\nu_{12}\nu_{21}} \ , \ Q_{22} = \frac{E_2}{1-\nu_{12}\nu_{21}} \ , \ Q_{12} = \frac{\nu_{12}E_1}{1-\nu_{12}\nu_{21}}$$

$$Q_{66} = G_{12} \ , \ Q_{44} = G_{23} \ , \ Q_{55} = G_{13} \quad (3.5)$$

E_i are Young's moduli; ν_{ij} are Poisson's ratios and G_{ij} are shear moduli, $\alpha_1$and $\alpha_2$are the coefficients of thermal expansion in the fiber direction and transverse direction respectively and thermal load across the thickness is assumed to be:

$$T(\mathrm{x},\mathrm{y},\mathrm{z}) = \mathrm{T}_1(x,y) + \frac{z}{h}T_2(x,y) + \frac{ft(z)}{h}T_3(x,y) \tag{3.6}$$

Where T_1 , T_2 , $and\ T_3$ are thermal loads and $ft(z) = \frac{h}{\pi}\sin\frac{\pi z}{h}$,the non-linear term associated with thermal load T_3 is the trigonometric function in terms of the thickness coordinate.

Since the laminated composite is composed of multiple orthotropic layers whose principal material axes may be arbitrarily oriented with respect to the global coordinate system of the laminate (x, y, z), the constitutive equations of each layer must be transformed from the local (material) axes to the global coordinate system. In this global system, the constitutive relations for any given layer k under the plane stress assumption can be expressed using the transformed reduced stiffness coefficients $\bar{Q}_{ij}$, as follows:

$$\begin{Bmatrix}\sigma_{xx}\\ \sigma_{yy}\\ \tau_{xy}\end{Bmatrix}_{(k)} = \begin{bmatrix}\overline{Q_{11}} & \overline{Q_{12}} & \overline{Q_{16}}\\ \overline{Q_{12}} & \overline{Q_{22}} & \overline{Q_{26}}\\ \overline{Q_{16}} & \overline{Q_{26}} & \overline{Q_{66}}\end{bmatrix}_{(\mathrm{k})} \begin{Bmatrix}\varepsilon_{xx}-\alpha_x T\\ \varepsilon_{yy}-\alpha_y T\\ \gamma_{xy}\end{Bmatrix}_{(k)}$$

$$\begin{Bmatrix}\tau_{yz}\\ \tau_{xz}\end{Bmatrix}_{(k)} = \begin{bmatrix}\overline{Q_{44}} & 0\\ 0 & \overline{Q_{55}}\end{bmatrix}_{(\mathrm{k})} \begin{Bmatrix}\gamma_{yz}\\ \gamma_{xz}\end{Bmatrix}_{(k)} \tag{3.7}$$

Where $\bar{Q}_{ij}$ are the transformed reduced material properties ,and are given as follows :

$$\begin{aligned}
\overline{Q_{11}} &= Q_{11}\cos^4\theta + 2(Q_{12}+2Q_{66})\sin^2\theta\cos^2\theta + Q_{22}\sin^4\theta\\
\overline{Q_{12}} &= (Q_{11}+Q_{22}-4Q_{66})\sin^2\theta\cos^2\theta + Q_{12}(\sin^4\theta+\cos^4\theta)\\
\overline{Q_{22}} &= Q_{11}\sin^4\theta + 2(Q_{12}+2Q_{66})\sin^2\theta\cos^2\theta + Q_{22}\cos^4\theta\\
\overline{Q_{16}} &= (Q_{11}-Q_{12}-2Q_{66})\cos^3\theta\sin\theta - (Q_{22}-Q_{12}-2Q_{66})\cos\theta\sin^3\theta\\
\overline{Q_{26}} &= (\mathrm{Q}_{11}-Q_{12}-2Q_{66})\cos\theta\sin^3\theta - (Q_{22}-Q_{12}-2Q_{66})\cos^3\theta\sin\theta\\
\overline{Q_{66}} &= (Q_{11}+Q_{22}-2Q_{12}-2Q_{66})\sin^2\theta\cos^2\theta + Q_{66}(\sin^4\theta+\cos^4\theta)\\
\overline{Q_{44}} &= Q_{44}\cos^2\theta + Q_{55}\sin^2\theta\\
\overline{Q_{55}} &= Q_{55}\cos^2\theta + Q_{44}\sin^2\theta
\end{aligned} \tag{3.8}$$

(Daniel & Ishai, 2006)

Where θ is the fiber orientation angle.

3.6. Governing Equations

The principle of virtual work is used in this study to derive the governing equations. It states that the total virtual work of internal forces equals that of external forces and it can be expressed by this formulation:

$$\delta \int_{t_1}^{t_2} (U - V)\,\mathrm{dt} = 0 \tag{3.9}$$

Where δU is the variation of the work of internal forces (strain energy) given by:

$$\delta U = \int_{-h/2}^{+h/2} \int_{A} (\sigma_{xx}\delta\varepsilon_{xx} + \sigma_{yy}\delta\varepsilon_{yy} + \tau_{xy}\delta\gamma_{xy} + \tau_{xz}\delta\gamma_{xz} + \tau_{yz}\delta\gamma_{yz})\,dz\,dA \tag{3.10}$$

And δV is the variation of the work of external forces given by:

$$\delta V = \int_{A} q\,\delta w_0\,dx\,dy \tag{3.11}$$

By substituting the variation of external work in Eq.(3.11) and the variation of the strain energy in Eq.(3.10) into the virtual work principle Eq.(3.9), and integrating the resulting equation by parts while collecting the coefficients of the virtual displacements, δu_0 , δv_0 , δw_0 , $\delta\theta_1$, $\delta\theta_2$, the governing differential equations are obtained as follows:

$$\delta u : \frac{\partial N_{xx}}{\partial x} + \frac{\partial N_{xy}}{\partial y} = 0$$

$$\delta v : \frac{\partial N_{yy}}{\partial y} + \frac{\partial N_{xy}}{\partial x} = 0$$

$$\delta w : \frac{\partial^2 M_{xx}}{\partial x^2} + 2\frac{\partial^2 M_{xy}}{\partial x \partial y} + \frac{\partial^2 M_{yy}}{\partial y^2} + q = 0 \tag{3.12}$$

$$\delta\theta_1 : \frac{\partial P_{xy}}{\partial y} + y^* \frac{\partial M_{xy}}{\partial y} + y^* \frac{\partial M_{xx}}{\partial x} + \frac{\partial P_{xx}}{\partial x} - K_1 - y^* Q_1 = 0$$

$$\delta\theta_2 : \frac{\partial P_{yy}}{\partial y} + y^* \frac{\partial M_{yy}}{\partial y} + y^* \frac{\partial M_{xy}}{\partial x} + \frac{\partial P_{xy}}{\partial x} - K_2 - y^* Q_2 = 0$$

Where q is the load term ,N_i , M_i , P_i , Q_i and K_i are the resultants of the following intergrations;

$$(\mathrm{N}_i, M_i, P_i) = \sum_{k=1}^{N} \int_{z_k}^{z_{k+1}} \sigma_i^{(k)}(1, z, \psi(\mathrm{z}))dz \ (i = 1,2,6) \tag{3.13}$$

$$(Q_1, \mathrm{K}_1) = \sum_{k=1}^{N} \int_{z_k}^{z_{k+1}} \sigma_5^{(k)}(1, g(z))dz \tag{3.14}$$

$$(Q_2, \mathrm{K}_2) = \sum_{k=1}^{N} \int_{z_k}^{z_{k+1}} \sigma_4^{(k)}(1, g(z))dz \tag{3.15}$$

$$\begin{gathered} N_1 = N_{xx} \ , \ N_2 = N_{yy} \ , \ N_6 = N_{xy} \\ M_1 = M_{xx} \ , \ M_2 = M_{yy} \ , \ M_6 = M_{xy} \\ P_1 = P_{xx} \ , \ P_2 = P_{yy} \ , \ P_6 = P_{xy} \end{gathered} \tag{3.16}$$

$$\sigma_1 = \sigma_{xx} \ , \ \sigma_2 = \sigma_{yy} \ , \ \sigma_6 = \tau_{xy} \ , \ \sigma_4 = \tau_{yz} \ , \ \sigma_5 = \tau_{xz} \tag{3.17}$$

The overall resultants in the laminate , are given by the difference between the contributions due to mechanical loading and those due to thermal as represented below :

$$\begin{aligned} N_{xx} &= N_{xx}^{M} - N_{xx}^{T} \\ N_{yy} &= N_{yy}^{M} - N_{yy}^{T} \\ M_{yy} &= M_{yy}^{M} - M_{yy}^{T} \\ M_{xx} &= M_{xx}^{M} - M_{xx}^{T} \\ P_{xx} &= P_{xx}^{M} - P_{xx}^{T} \\ P_{yy} &= P_{yy}^{M} - P_{yy}^{T} \end{aligned} \tag{3.18}$$

The differential governing equations are represented in terms of the laminate stiffness matrix coefficients as follows:

$$\begin{aligned} &\delta u : -A_{11}\frac{\partial^2 u_0}{\partial x^2} - A_{66}\frac{\partial^2 u_0}{\partial y^2} - (\mathrm{A}_{12} + A_{66})\frac{\partial^2 v_0}{\partial x \partial y} + B_{11}\frac{\partial^3 w_0}{\partial x^3} + (B_{12} + 2B_{66})\frac{\partial^3 w_0}{\partial x \partial y^2} - y^* B_{11}\frac{\partial^2 \theta_1}{\partial x^2} - E_{11}\frac{\partial^2 \theta_1}{\partial x^2} \\ &- y^* B_{66}\frac{\partial^2 \theta_1}{\partial y^2} - E_{66}\frac{\partial^2 \theta_1}{\partial y^2} - (y^* B_{12} + E_{12} + y^* B_{66} + E_{66})\frac{\partial^2 \theta_2}{\partial x \partial y} \\ &-(\mathrm{L}_{11}^{T} + L_{21}^{T})\frac{\partial T_1}{\partial x} - (P_{11} + P_{21})\frac{\partial T_2}{\partial x} - (R_{11} + R_{21})\frac{\partial T_3}{\partial x} = 0 \end{aligned} \tag{3.19}$$

$$\delta v: -(A_{11}+A_{66})\frac{\partial^2 u_0}{\partial x\partial y}-A_{22}\frac{\partial^2 v_0}{\partial y^2}-A_{66}\frac{\partial^2 v_0}{\partial x^2}+B_{12}\frac{\partial^3 w_0}{\partial x^2\partial y}+B_{22}\frac{\partial^3 w_0}{\partial y^3}$$
$$+2B_{66}\frac{\partial^3 w_0}{\partial x^2\partial y}-(y^*B_{12}+E_{12}+y*B_{66}+E_{66})\frac{\partial^2\theta_1}{\partial x\partial y}-(y^*B_{22}+E_{22})\frac{\partial^2\theta_2}{\partial y^2}-(y^*B_{66}+E_{66})\frac{\partial^2\theta_2}{\partial x^2}$$
$$-(L_{12}^T+L_{22}^T)\frac{\partial T_1}{\partial y}-(P_{12}+P_{22})\frac{\partial T_2}{\partial y}-(R_{11}+R_{22})\frac{\partial T_3}{\partial y}=0 \tag{3.20}$$

$$\delta w: B_{11}\frac{\partial^3 u_0}{\partial x^3}+(2B_{66}+B_{12})\frac{\partial^3 u_0}{\partial x\partial y^2}+(B_{12}+2B_{66})\frac{\partial^3 v_0}{\partial x^2\partial y}+B_{22}\frac{\partial^3 v_0}{\partial y^3}-D_{11}\frac{\partial^4 w_0}{\partial x^4}-(2D_{12}+4D_{66})\frac{\partial^4 w_0}{\partial x^2\partial y^2}$$
$$-D_{22}\frac{\partial^4 w_0}{\partial y^4}+(y^*D_{11}+F_{11})\frac{\partial^3\theta_1}{\partial x^3}+(y^*2D_{66}+2F_{66}+y^*D_{12}+F_{12})\frac{\partial^3\theta_1}{\partial x\partial y^2}+(y^*D_{12}+F_{12}+y*2\mathrm{D}_{66}+2F_{66})\frac{\partial^3\theta_2}{\partial x^2\partial y}$$
$$+(y^*D_{22}+F_{22})\frac{\partial^3\theta_2}{\partial y^3}+(S_{11}+S_{21})\frac{\partial^2 T_1}{\partial x^2}+(S_{12}+S_{22})\frac{\partial^2 T_1}{\partial y^2}+(T_{11}+T_{21})\frac{\partial^2 T_2}{\partial x^2}+(T_{12}+T_{22})\frac{\partial^2 T_2}{\partial y^2}+(U_{11}+U_{21})\frac{\partial^2 T_3}{\partial x^2}$$
$$+(\mathrm{U}_{12}+U_{22})\frac{\partial^2 T_3}{\partial y^3}+q=0 \tag{3.21}$$

$$\delta\theta_1: -(E_{66}+y^*B_{66})\frac{\partial^2 u_0}{\partial y^2}-(y^*B_{11}+E_{11})\frac{\partial^2 u_0}{\partial x^2}+(2\mathrm{F}_{66}+y*2\mathrm{D}_{66}+y^*D_{12}+F_{12})\frac{\partial^3 w_0}{\partial x\partial y^2}+(\mathrm{y}*D_{11}+F_{11})\frac{\partial^3 w_0}{\partial x^3}$$
$$-(E_{66}+y^*B_{66}+E_{12})\frac{\partial^2 v_0}{\partial x\partial y}-(y^*F_{66}+H_{66}+(y^*)^2D_{66}+y^*F_{66})\frac{\partial^2\theta_1}{\partial y^2}-((y^*)^2D_{11}+y^*2F_{11}+H_{11})\frac{\partial^2\theta_1}{\partial x^2}$$
$$-(y^*F_{66}+H_{66}+(y^*)^2D_{66}+y^*2F_{66}+(y^*)^2D_{12}+y^*2F_{12}+H_{12})\frac{\partial^2\theta_2}{\partial x\partial y}-(A_{55}(y^*)^2+y^*2J_{55}+L_{55})\theta_1$$
$$-(y^*S_{11}+y^*S_{21}+V_{11}+V_{21})\frac{\partial T_1}{\partial x}-(y^*T_{11}+y^*T_{21}+W_{11}+W_{21})\frac{\partial T_2}{\partial x}-(y^*U_{11}+y^*U_{21}+X_{11}+X_{21})\frac{\partial T_3}{\partial x}=0 \tag{3.22}$$

$$\delta\theta_2: -(y^*B_{12}+y^*B_{66}+E_{12}+E_{66})\frac{\partial^2 u_0}{\partial x\partial y}-(y^*B_{22}+E_{22})\frac{\partial v_0}{\partial y^2}$$
$$-(y^*B_{66}+E_{66})\frac{\partial^2 v_0}{\partial x^2}+(y^*D_{12}+y^*2D_{66}+F_{12}+2F_{66})\frac{\partial^3 w_0}{\partial x^2\partial y}$$
$$+(y^*D_{22}+F_{22})\frac{\partial^3 w_0}{\partial y^3}-((y^*)^2D_{12}+y^*2F_{12}+(y^*)^2D_{66}+y^*2F_{66}+H_{12}+H_{66})\frac{\partial^2\theta_1}{\partial x\partial y} \tag{3.23}$$
$$-((y^*)^2D_{22}+y^*2F_{22}+H_{22})\frac{\partial^2\theta_2}{\partial y^2}$$
$$-((y^*)^2D_{66}+y^*2F_{66}+H_{66})\frac{\partial^2\theta_2}{\partial x^2}-((y^*)^2A_{44}+y^*2J_{44}+L_{44})\theta_2-(y^*S_{12}+y^*S_{22}+V_{12}+V_{22})\frac{\partial T_1}{\partial y}$$
$$-(y^*T_{12}+y^*T_{22}+W_{12}+W_{22})\frac{\partial T_2}{\partial y}-(y^*U_{12}+y^*U_{22}+X_{12}+X_{22})\frac{\partial T_3}{\partial y}=0$$

The laminate stiffness coefficients A_{ij} , B_{ij}….etc in the above equations are expressed in terms of reduced stiffness coefficients $\overline{Q_{ij}}$ as follows:

$$A_{ij} = \int_{-h/2}^{h/2} \overline{Q}_{ij}^{(k)} dz \ (i = 1,2,4,5,6) \tag{3.24}$$

$$(\mathrm{B}_{ij}, D_{ij}, E_{ij}, F_{ij}, H_{ij}) = \int_{-h/2}^{h/2} \overline{Q}_{ij}^{(k)} (z, z^2, \psi(z), z\psi(z), \psi^2(z)) dz \ (i = 1,2,6) \tag{3.25}$$

$$(\mathrm{J}_{ij}) = \int_{-h/2}^{h/2} \overline{Q}_{ij}^{(k)} \, \mathrm{g}(z) dz \ (i = 4,5) \tag{3.26}$$

$$(\mathrm{L}_{ij}) = \int_{-h/2}^{h/2} \overline{Q}_{ij}^{(k)} \, \mathrm{g}^2(z) dz \ (i = 4,5) \tag{3.27}$$

$$(L_{ij}^T, P_{ij}, R_{ij}) = \sum_{k=1}^{N} \int_{z_k}^{z_{k+1}} \alpha_i^{(k)} \overline{Q}_{ij}^{(k)} (1, z/h, ft(z)/h) \ (i = 1,2) \tag{3.28}$$

$$(\mathrm{S}_{ij}, \mathrm{T}_{ij}, \mathrm{U}_{ij}) = \sum_{k=1}^{N} \int_{z_k}^{z_{k+1}} \alpha_i^{(k)} \overline{Q}_{ij}^{(k)} (\mathrm{z}, z^2/h, ft(z)\mathrm{z}/h)^{(i=1,2)} \tag{3.29}$$

$$(\mathrm{V}_{ij}, \mathrm{W}_{ij}, \mathrm{X}_{ij}) = \sum_{k=1}^{N} \int_{z_k}^{z_{k+1}} \alpha_i^{(k)} \overline{Q}_{ij}^{(k)} \psi(\mathrm{z})(1, z/h, ft(z)/h)^{(i=1,2)} \tag{3.30}$$

With:

$A_{i6} = B_{i6} = D_{i6} = E_{i6} = F_{i6} = H_{i6} = 0 \ (i = 1,2)$

$A_{45} = J_{45} = L_{45} = 0$

3.7. Analytical Solutions for a Simply Supported Laminated Plate

The analytical solution of the partial differential equations can be obtained using Navier's method, which is commonly applied in the bending analysis of simply supported laminated composite plates.

The boundary conditions for simply supported edges are:

$$u_0 = w_0 = \theta_1 = N_{yy} = M_{yy} = 0 \text{ at } y=0,b$$
$$v_0 = w_0 = \theta_2 = N_{xx} = M_{xx} = 0 \text{ at } x=0,a \tag{3.31}$$

The displacement coefficients can be expressed in the following form:

$$u(x,y) = \sum_{m=1}^{\infty}\sum_{n=1}^{\infty} U_{mn} \cos(\alpha x)\sin(\beta y)$$

$$\mathrm{v}(x,y) = \sum_{m=1}^{\infty}\sum_{n=1}^{\infty} V_{mn} \sin(\alpha x)\cos(\beta y)$$

$$\mathrm{w}(x,y) = \sum_{m=1}^{\infty}\sum_{n=1}^{\infty} W_{mn} \sin(\alpha x)\sin(\beta y) \tag{3.32}$$

$$\theta_1(x,y) = \sum_{m=1}^{\infty}\sum_{n=1}^{\infty} \theta^1{}_{mn} \cos(\alpha x)\sin(\beta y)$$

$$\theta_2(x,y) = \sum_{m=1}^{\infty}\sum_{n=1}^{\infty} \theta^2{}_{mn} \sin(\alpha x)\cos(\beta y)$$

Where : $\alpha = \frac{m\pi}{a}$ and $\beta = \frac{m\pi}{b}$ and U_{mn} , V_{mn} , W_{mn} , θ^1_{mn} , θ^2_{mn} are the unknown Fourier coefficients to be determined for each pair of integers (*m,n*).

Thermal load is expanded in double Fourier sine series as follows:

$$T_1(x,y) = \sum_{m=1}^{\infty}\sum_{n=1}^{\infty} T_{1mn} \sin(\alpha x)\sin(\beta \mathrm{y})$$
$$T_2(x,y) = \sum_{m=1}^{\infty}\sum_{n=1}^{\infty} T_{2mn} \sin(\alpha x)\sin(\beta \mathrm{y}) \tag{3.33}$$
$$T_3(x,y) = \sum_{m=1}^{\infty}\sum_{n=1}^{\infty} T_{3mn} \sin(\alpha x)\sin(\beta \mathrm{y})$$

For single sinusodial thermal load (m=n=1), series coefficients lead to $T_{1mn} = T_{2mn} = T_{3mn} = T_0$ where T_0 is the maximum intensity of thermal load.

Q_{mn} is the coefficient in the double Fourier expansion of the transverse load.

$$q(x,y)=\sum_{m=1}^{\infty}\sum_{n=1}^{\infty}Q_{mn}\sin(\alpha x)\sin(\beta \mathrm{y}) \tag{3.34}$$

For single sinusodial mechanical load (m=n=1), series coefficients lead to $Q_{mn}=q_0$ whereq_0 is the maximum intensity of mechanical load.

By substituting these solutions into the governing equations of movement, the following matrix form is formed:

$$[K]\{\Delta\}=\{F\} \tag{3.35}$$

$[K]$ is the stiffness matrix and can be represented in this form:

$$[K]=\begin{bmatrix} k_{11} & k_{12} & k_{13} & k_{14} & k_{15} \\ k_{21} & k_{22} & k_{23} & k_{24} & k_{25} \\ k_{31} & k_{32} & k_{33} & k_{34} & k_{35} \\ k_{41} & k_{42} & k_{43} & k_{44} & k_{45} \\ k_{51} & k_{52} & k_{53} & k_{54} & k_{55} \end{bmatrix} \tag{3.36}$$

Where the elements of the stiffness matrix are as follows:

$$\begin{aligned}
k_{11} &= -A_{11}\alpha^2 - A_{66}\beta^2 \\
k_{12} &= -A_{12}\alpha\beta - A_{66}\alpha\beta \\
k_{13} &= B_{11}\alpha^3 + B_{12}\alpha\beta^2 + 2B_{66}\alpha\beta^2 \\
k_{14} &= -y^* B_{11}\alpha^2 - E_{11}\alpha^2 - y^* B_{66}\beta^2 - E_{66}\beta^2 \\
k_{15} &= -y^* B_{12}\alpha\beta - y^* B_{66}\alpha\beta - E_{66}\alpha\beta - E_{12}\alpha\beta \\
k_{12} &= k_{21} \\
k_{22} &= -A_{22}\beta^2 - A_{66}\alpha^2 \\
k_{23} &= B_{12}\alpha^2\beta + B_{22}\beta^3 + 2B_{66}\alpha^2\beta \\
k_{24} &= -y^* B_{12}\alpha\beta - E_{12}\alpha\beta - y^* B_{66}\alpha\beta - E_{66}\alpha\beta \\
k_{25} &= -y^* B_{22}\beta^2 - E_{22}\beta^2 - E_{66}\alpha^2 - y^* B_{66}\alpha^2 \\
k_{31} &= k_{13} \\
k_{32} &= k_{23}
\end{aligned} \tag{3.37}$$

$$k_{33} = -D_{11}\alpha^4 - D_{12}\alpha^2\beta^2 - 4D_{66}\alpha^2\beta^2 - D_{12}\alpha^2\beta^2 - D_{22}\beta^4$$

$$k_{34} = y^* D_{11}\alpha^3 + F_{11}\alpha^3 + y^* 2D_{66}\alpha\beta^2 + 2F_{66}\alpha\beta^2 + y^* D_{12}\alpha\beta^2 + F_{12}\alpha\beta^2$$

$$k_{35} = y^* D_{12}\alpha^2\beta + F_{12}\alpha^2\beta + y^* 2D_{66}\alpha^2\beta + 2F_{66}\alpha^2\beta + y^* D_{22}\beta^3 + F_{22}\beta^3$$

$$k_{41} = k_{14}$$

$$k_{42} = k_{24}$$

$$k_{43} = k_{34}$$

$$k_{44} = -y*2F_{66}\beta^2 - H_{66}\beta^2 - (y^*)^2 D_{66}\beta^2 - (y^*)^2 D_{11}\alpha^2 - y^* 2F_{11}\alpha^2 - H_{11}\alpha^2 - y^* 2J_{55} - L_{55} - (y^*)^2 A_{55}$$

$$k_{45} = -y^* 2F_{66}\alpha\beta - y^* 2F_{12}\alpha\beta - (y^*)^2 D_{12}\alpha\beta - (y^*)^2 D_{66}\alpha\beta - H_{66}\alpha\beta - H_{12}\alpha\beta$$

$$k_{51} = k_{15}$$

$$k_{52} = k_{25}$$

$$k_{53} = k_{35}$$

$$k_{54} = k_{45}$$

$$k_{55} = -y^* 2F_{22}\beta^2 - y^* 2F_{66}\alpha^2 - (y^*)^2 D_{66}\alpha^2 - (y^*)^2 D_{22}\beta^2 - H_{22}\beta^2 - H_{66}\alpha^2 - (y^*)^2 A_{44} - y^* 2J_{44} - L_{44}$$

$\{\Delta\}$ is the generalised displacement vector and is expressed as follows:

$$\{\Delta\} = \{U_{mn}, V_{mn}, W_{mn}, \theta^1_{mn}, \theta^2_{mn}\}^T \tag{3.38}$$

$\{F\}$ is the force vector and is expressed as follows:

$$\{F\} = \{F_1, F_2, F_3, F_4, F_5\}^T \tag{3.39}$$

Where the elements of the force vector are as follows:

$$\begin{aligned}
F_1 &= \alpha(L^T_{11} + L^T_{22})T_{1mn} + \alpha(\mathrm{P}_{11} + P_{21})T_{2mn} + \alpha(R_{11} + R_{21})T_{3mn} \\
F_2 &= \alpha(L^T_{12} + L^T_{22})T_{1mn} + \alpha(\mathrm{P}_{12} + P_{22})T_{2mn} + \alpha(R_{12} + R_{22})T_{3mn} \\
F_3 &= -Q_{mn} - (\alpha^2(S_{11} + S_{21}) + \beta^2(S_{12} + S_{22}))T_{1mn} - (\alpha^2(T_{11} + T_{21}) + \beta^2(T_{12} + T_{22}))T_{2mn} - (\alpha^2(U_{11} + U_{21}) + \beta^2(U_{12} + U_{22}))T_{3mn} \\
F_4 &= \alpha(y^*(\mathrm{S}_{11} + S_{21}) + V_{11} + V_{21})T_{1mn} + \alpha(y^*(T_{11} + T_{21}) + W_{11} + W_{21})T_{2mn} + \alpha(y^*(U_{11} + U_{21}) + X_{11} + X_{21})T_{3mn} \\
F_5 &= \beta(y^*(S_{12} + S_{22}) + V_{12} + V_{22})T_{1mn} + \beta(y^*(T_{12} + T_{22}) + W_{12} + W_{22})T_{2mn} + \beta(y^*(U_{12} + U_{22}) + X_{12} + X_{22})T_{3mn}
\end{aligned} \tag{3.40}$$

3.8. Conclusion

In this chapter, a comprehensive mathematical formulation was developed to model the static behaviour of laminated composite plates under thermal loading. A refined displacement field was introduced to better capture the response of cross-ply laminates. The governing equations were derived using established variational principles, and the laminate stiffness matrices were used to express the structural behaviour in a compact and systematic form.

To obtain analytical solutions, Navier's method was employed, which allowed for the exact satisfaction of simply supported boundary conditions and enabled the determination of displacement and stress distributions under thermal effects.

These formulations form the theoretical foundation for the results and analyses presented in the subsequent chapter, where the performance and accuracy of the proposed model are further examined.

Chapter 4 :
RESULTS ,DISCUSSION AND CONCLUSION

4.1. Introduction

This chapter presents the results and discussion of the static behavior of cross-ply laminated composite plates subjected to non-linear thermal loading, using a refined displacement field. The study evaluates transverse deflection ($\overline{w}$) and stresses under various influencing parameters, including the aspect ratio (a/h), material anisotropy ratio (E_1/E_2), and thermal expansion ratio (α_2/α_1). The composite laminates considered are orthotropic and modeled as [0°], [0°/90°], and [0°/90°/0°] configurations with simply supported boundary conditions. The governing equations were derived using the principle of virtual work and solved using the Navier-type solution procedure implemented in MAPLE 12. Numerical results are presented and discussed in detail, highlighting the influence of lamination sequence and material anisotropy on the deflection response under thermal effects. Comparative observations are also made with respect to findings from existing literature, to validate the accuracy and effectiveness of the proposed displacement model.

4.1.1. Characteristics of Materials used

The thickness and material properties of all the layers are assumed to be identical. In the analysis, the elastic properties of the laminas are assumed to be:

$$\frac{E_1}{E_2} = 25\ ; \qquad G_{12} = G_{13} = 0.5E_2\ ; \qquad G_{23} = 0.2E_2\ ; \qquad \nu_{12} = 0.25\ ; \qquad \frac{\alpha_2}{\alpha_1} = 3$$

E represents the Young's modulus ,ν denotes Poisson's ratio ,and *G* the shear modulus.α_1 is coefficient of thermal expansion in the direction of fiber and α_2 is coefficient of thermal expansion in the transverse direction.The laminated plate has dimensions defined by its length ***a***, width ***b***, and thickness ***h***. In this study, ***b*** = ***a*****,** indicating that the plate is square.

- **The Non-dimensional formulas**

The following relations are used for the presentation of the non-dimensional fundamental deflection and stresses :

$$\overline{w} = w\left(\frac{a}{b}, \frac{b}{2}, 0\right)\frac{10 \times h}{\alpha_1 T_0 b^2}\ ;\ \overline{\sigma_{xx}} = \sigma_{xx}\left(\frac{a}{2}, \frac{b}{2}, -\frac{h}{2}\right)\frac{1}{\alpha_1 T_0 a^2 E_2}\ ;\ \overline{\sigma_{yy}} = \sigma_{yy}\left(\frac{a}{2}, \frac{b}{2}, -\frac{h}{2}\right)\frac{1}{\alpha_1 T_0 E_2 a^2}$$

$$\overline{\tau_{xy}} = \tau_{xy}\left(0,0,-\frac{h}{2}\right)\frac{1}{\alpha_1 T_0 E_2 a^2}\ ;$$

$$\overline{\tau_{yz}} = \tau_{yz}\left(\frac{a}{2},0,z\right)\frac{1}{\alpha_1 T_0 E_2 a^2}\ ;\ \overline{\tau_{xz}} = \tau_{xz}\left(0,\frac{b}{2},z\right)\frac{1}{\alpha_1 T_0 E_2 a^2}$$

4.2. Validation of the Present Theory

The performance of the present refined shear deformation theory was evaluated by comparing the obtained results with those generated using the Classical Plate Theory (CPT), First-Order Shear Deformation Theory (FSDT), Higher-Order Shear Deformation Theory (HSDT), and the trigonometric theory (Ghugal & Kulkarni, 2013). The laminated plates were subjected to non-linear thermal load *(*$T_1 = 0, T_2 = T_3 = T_0 = 1$). The assessment was based on the predicted values of non-dimensional transverse deflection ($\bar{w}$), in-plane normal stresses ($\overline{\sigma_{xx}}$, $\overline{\sigma_{yy}}$), in-plane shear stress ($\overline{\tau_{xy}}$), and transverse shear stresses ($\overline{\tau_{xz}}$, $\overline{\tau_{yz}}$) for aspect ratios a/h = 4 and a/h = 10.

Table 1:Results for (0°/90°/0°)Laminate

a/h	Theories	$\bar{w}$	$\overline{\sigma_{xx}}$	$\overline{\sigma_{yy}}$	$\overline{\tau_{xy}}$	$\overline{\tau_{xz}}$	$\overline{\tau_{yz}}$
4	Present	1.9415	-1.5979	1.4089	0.9631	0.0430	-0.1190
	HSDT	1.9415	-1.5985	1.4090	0.9631	0.0430	-0.1189
	CPT	1.8293	-1.7269	1.5349	0.9027	0.1140	-0.1538
	FSDT	1.9463	-1.2646	1.3781	0.9734	0.0461	-0.1141
	Trigonometric (Ghulgal &Kulkarni, 2013)	1.9405	-1.6163	1.4118	0.9620	0.0384	-0.1212
10	Present	1.8599	-1.6977	1.5024	0.9183	0.0383	-0.0580
	HSDT	1.8599	-1.6979	1.5025	0.9183	0.0383	-0.0579
	CPT	1.8293	-1.7269	1.5349	0.9027	0.0456	-0.0615
	FSDT	1.8583	-1.6103	1.4960	0.9203	0.0388	-0.0575
	Trigonometric (Ghulgal &Kulkarni, 2013)	1.8599	-1.7015	1.5030	0.9189	0.0369	-0.0588

Table 2:Results for (0°/90°)Laminate

a/h	Theories	$\bar{w}$	$\overline{\sigma_{xx}}$	$\overline{\sigma_{yy}}$	$\overline{\tau_{xy}}$	$\overline{\tau_{xz}}$	$\overline{\tau_{yz}}$
4	Present	1.9506	-2.0980	1.3906	0.9797	-0.1249	-0.1250
	HSDT	1.9500	-2.0955	1.3904	0.9797	-0.1249	-0.1249
	CPT	1.9898	-2.1765	1.3884	0.9819	-0.1262	-0.1262
	FSDT	1.9899	-2.1765	1.3884	0.9820	-0.1262	-0.1262
	Trigonometric (Ghulgal &Kulkarni, 2013)	1.9460	-2.0811	1.3905	0.9794	-0.1246	-0.1246
10	Present	1.9835	-2.1645	1.3888	0.9815	-0.0503	-0.0504
	HSDT	1.9833	-2.1633	1.3888	0.9816	-0.0503	-0.0503

	CPT	1.9898	-2.1765	1.3884	0.9819	-0.0504	-0.0504
	FSDT	1.9899	-2.1765	1.3884	0.9820	-0.0504	-0.0504
	Trigonometric (Ghulgal &Kulkarni, 2013)	1.9827	-2.1609	1.3887	0.9816	-0.0504	-0.0504

Table 3:Results for (0°)Laminate

a/h	Theories	$\bar{w}$	$\overline{\sigma_{xx}}$	$\overline{\sigma_{yy}}$	$\overline{\tau_{xy}}$	$\overline{\tau_{xz}}$	$\overline{\tau_{yz}}$
4	Present	1.8958	-1.5355	1.3574	0.9876	0.0071	-0.1190
	HSDT	1.8957	-1.6251	1.4518	0.9423	0.0070	-0.1190
	CPT	1.8293	-1.7269	1.5349	0.9027	0.0754	-0.1797
	FSDT	1.9279	-1.3164	1.3224	1.0018	0.0143	-0.1186
	Trigonometric (Ghulgal &Kulkarni, 2013)	1.8919	-1.5424	1.3607	0.9862	0.0066	-0.1191
10	Present	1.8470	-1.6873	1.4935	0.9226	0.0237	-0.0663
	HSDT	1.8469	-1.7120	1.5018	0.9189	0.0237	-0.0662
	CPT	1.8293	-1.7269	1.5349	0.9027	0.0301	-0.0719
	FSDT	1.8520	-1.6323	1.4859	0.9256	0.0245	-0.0662
	Trigonometric (Ghulgal &Kulkarni, 2013)	1.8464	-1.6898	1.4943	0.9223	0.0237	-0.0663

For the [0°/90°/0°] laminate, values of ($\bar{w}$) predicted by the present theory, HSDT, FSDT, and the trigonometric theory were in close agreement, while CPT showed slight deviation due to the neglect of transverse shear effects. In the [0°/90°] configuration, the present theory, HSDT, and trigonometric theory produced similar deflections, while FSDT and CPT overpredicted ($\bar{w}$) at a/h = 4; all theories converged at a/h = 10. For the [0°] laminate, good agreement was observed among the present, HSDT, and trigonometric theories, while FSDT showed noticeably higher deflection at a/h = 4, and CPT remained slightly different across both aspect ratios.

In-plane stress ($\overline{\sigma_{xx}}$, $\overline{\sigma_{yy}}$) results for all laminates and both aspect ratios showed close alignment among the present theory, HSDT, and the trigonometric model. CPT generally overestimated in-plane stresses, while FSDT produced slightly lower values. For in-plane shear stress ($\overline{\tau_{xy}}$), the present theory, HSDT, and the trigonometric theory yielded very similar predictions. CPT significantly underpredicted ($\overline{\tau_{xy}}$), whereas FSDT tended to overpredict it, particularly at a/h=4.

For transverse shear stresses ($\overline{\tau_{xz}}$, $\overline{\tau_{yz}}$), further comparisons were made. For the [0°/90°/0°] laminate at a/h = 4, the present theory and HSDT produced nearly identical values for both shear components. The trigonometric theory showed slightly lower values for $\overline{\tau_{xz}}$, while FSDT

was slightly higher. CPT exhibited exaggerated results for both $\overline{\tau_{xz}}$ *and* $\overline{\tau_{yz}}$. At a/h = 10, the present theory, HSDT, trigonometric theory, and FSDT all gave similar values, with CPT continuing to overestimate. For the [0°/90°] laminate, all theories showed close agreement for both shear components at a/h = 10, while at a/h = 4, the refined theories agreed exactly, and CPT and FSDT were slightly higher but still within reasonable range. For the [0°] laminate, the present theory, HSDT, and trigonometric theory gave similar results for both $\overline{\tau_{xz}}$ *and* $\overline{\tau_{yz}}$. FSDT predicted slightly higher $\overline{\tau_{xz}}$, while CPT remained exaggerated in both components, especially at lower aspect ratios.

Overall, these results demonstrate that the present theory provides accurate and consistent predictions for deflection and stress behavior in laminated composite plates, showing excellent agreement with established higher-order and trigonometric shear deformation theories, and outperforming lower-order models such as CPT and FSDT, particularly under thermal loading.

4.3. Parametric Study

4.3.1. Effect of Aspect Ratio (a/h)

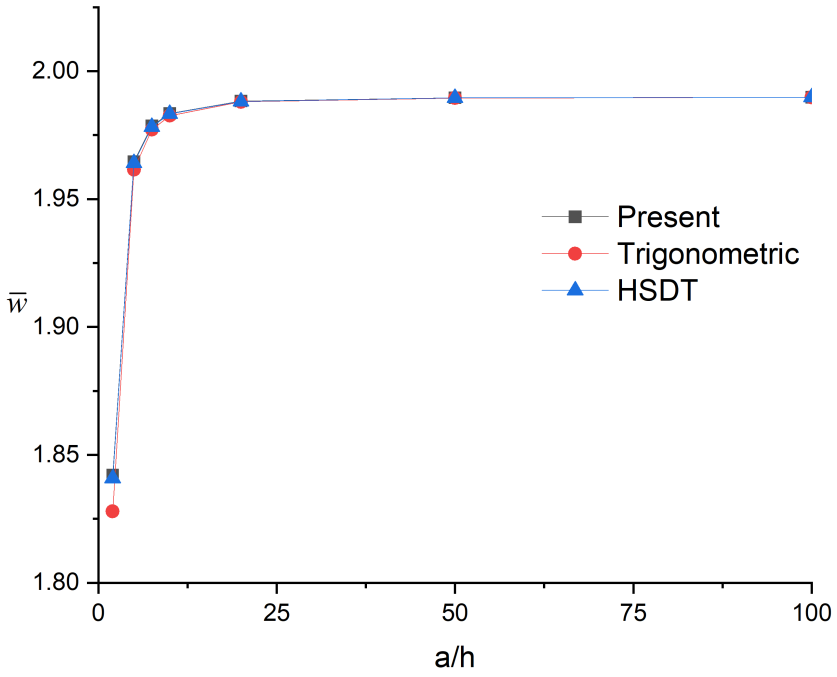

Figure 24:Variation of Non-dimensional deflection with Aspect Ratio for (0°/90°) laminate

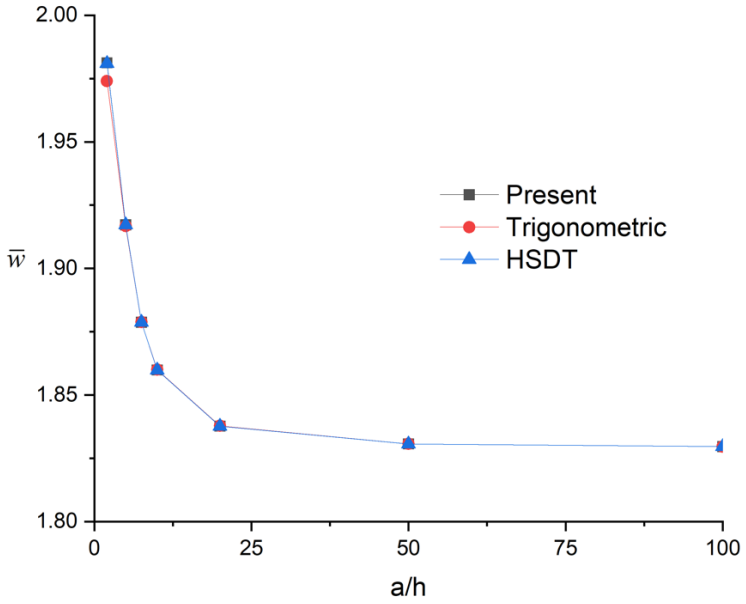

Figure 25:Variation of Non-dimensional Deflection with Aspect Ratio for (0°/90°/0°)Laminate

To investigate the influence of aspect ratio (*a/h*) on non-dimensional central deflection ($\overline{w}$), a constant stiffness ratio of $E_1/E_2 = 25$ was used, with a/h varied from 2 to 100. Results were obtained using the present refined theory, the Trigonometric theory (Ghugal & Kulkarni, 2013), and the Higher-Order Shear Deformation theory (HSDT) for comparison. For the symmetric [0°/90°/0°] laminate, the three theories produced consistent results, showing that $\overline{w}$ decreased with increasing *a/h*, and eventually approached a constant value. This trend reflects the reduced influence of transverse shear deformation as the plate becomes thinner. For the antisymmetric [0°/90°] laminate, similar consistency among the theories was observed. In this case, $\overline{w}$ increased with *a/h* at first and then stabilized at a constant value. This behavior is attributed to the bending-extension coupling effects present in antisymmetric laminates, which dominate at moderate thicknesses but diminish as shear deformation effects disappear at larger *a/h*. These findings confirm the capability of the present theory to accurately capture the deflection behavior of both symmetric and antisymmetric laminates across a wide range of aspect ratios.

4.3.2. Effect of Material Anisotropy (E_1/E_2)

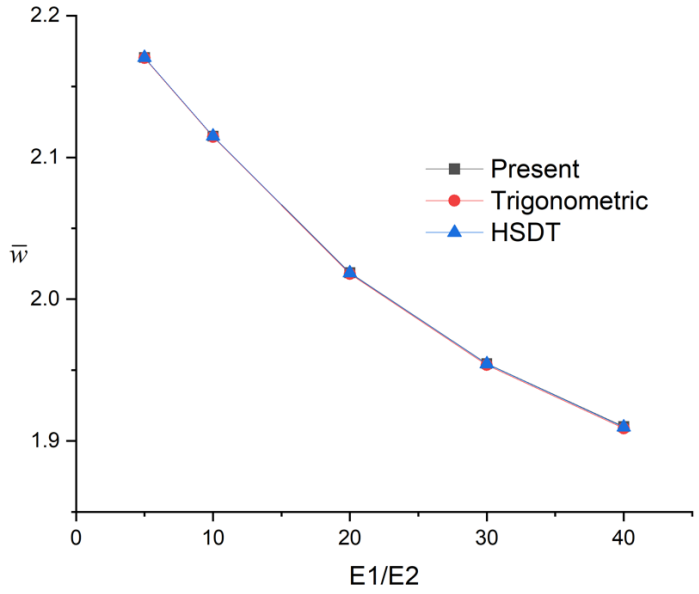

Figure 26:Variation of non-dimensional deflection with stiffness ratio E_1/E_2 for (0°/90°)Laminate

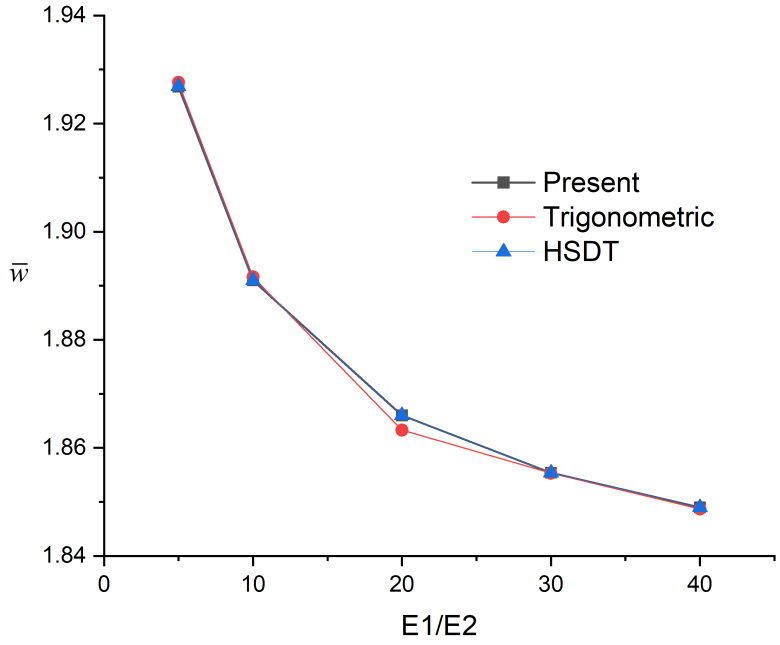

Figure 27:Variation of non-dimensional deflection with material anisotropy E_1/E_2 for (0°/90°/0°)Laminate

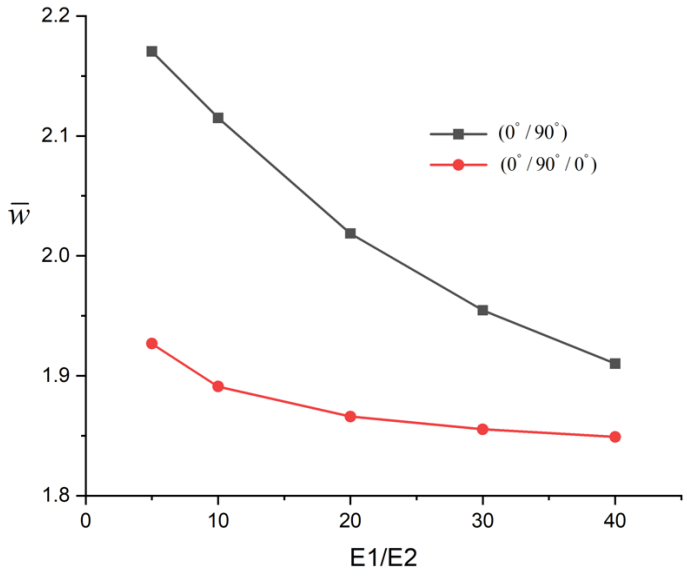

Figure 28:Comparison between stiffness ratio of (0°/90°)Laminate and (0°/90°/0°)Laminate

The influence of the ratio E_1/E_2, which characterizes material anisotropy, on the non-dimensional deflection $\overline{w}$ was investigated using the Present theory, the Trigonometric theory (Ghugal & Kulkarni,2013), and the Higher-Order Shear Deformation Theory (HSDT). The analysis was carried out for two laminate configurations: [0°/90°] and [0°/90°/0°], with a constant aspect ratio a/h = 10, while the material anisotropy ratio E_1/E_2 was varied from 5 to 40.

For the [0°/90°] laminate, all three theories showed excellent agreement, producing nearly identical values of $\overline{w}$ across the full range of material anisotropy ratios. A consistent trend was observed where $\overline{w}$ decreased with increasing E_1/E_2, indicating that greater stiffness in the fiber direction leads to reduced deflection. For the [0°/90°/0°] laminate, the present theory and HSDT yielded identical results, while the trigonometric theory produced slightly lower values at certain points but followed a similar overall trend.

Additionally, when comparing the two laminate types using the Present theory, it was observed that the [0°/90°] configuration exhibited higher values of $\overline{w}$ than the [0°/90°/0°] laminate at each ratio of material anisotropy. This is attributed to the added stiffness and symmetry of the [0°/90°/0°] laminate, which provides greater resistance to bending. Overall, the results confirm that increasing material anisotropy through higher E_1/E_2 values lead to a significant reduction in deflection, and the present theory accurately captures this behavior in line with established higher-order models.

4.3.3. Effect of Thermal Expansion Coefficient Ratio α_2/α_1

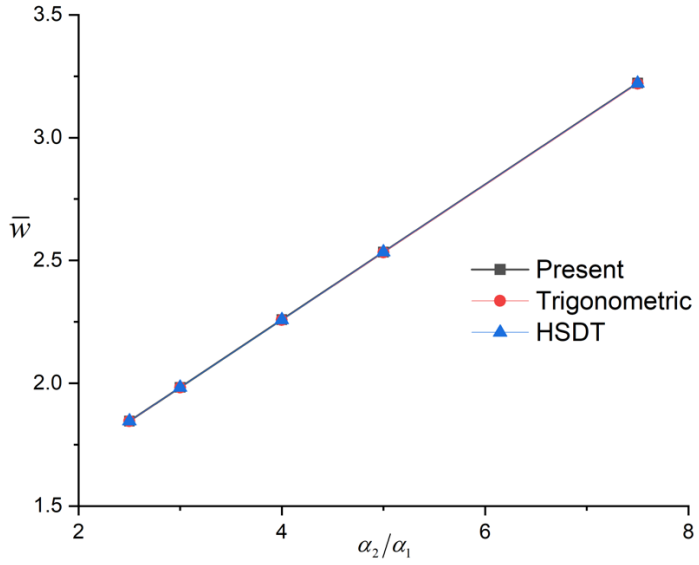

Figure 29: Variation of non-dimensional deflection with thermal expansion coefficient ratio for (0°/90°)Laminate

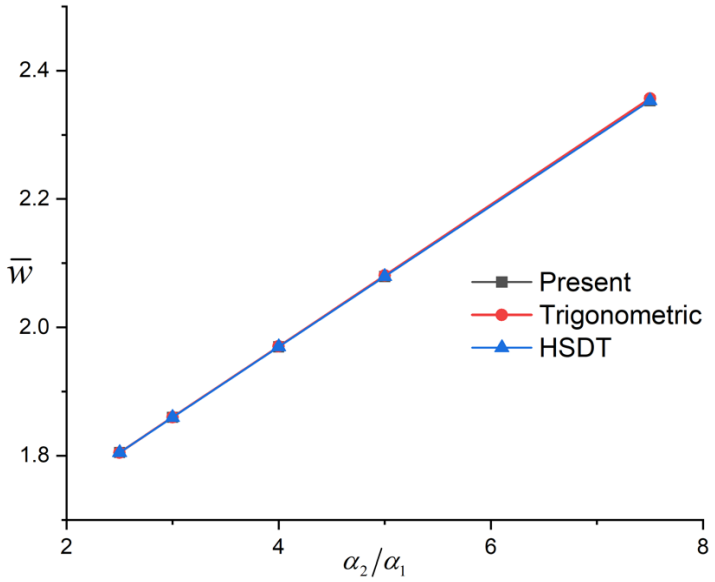

Figure 30:Variation of non-dimensional deflection with thermal expansion coefficient ratio for (0°/90°/0°)Laminate

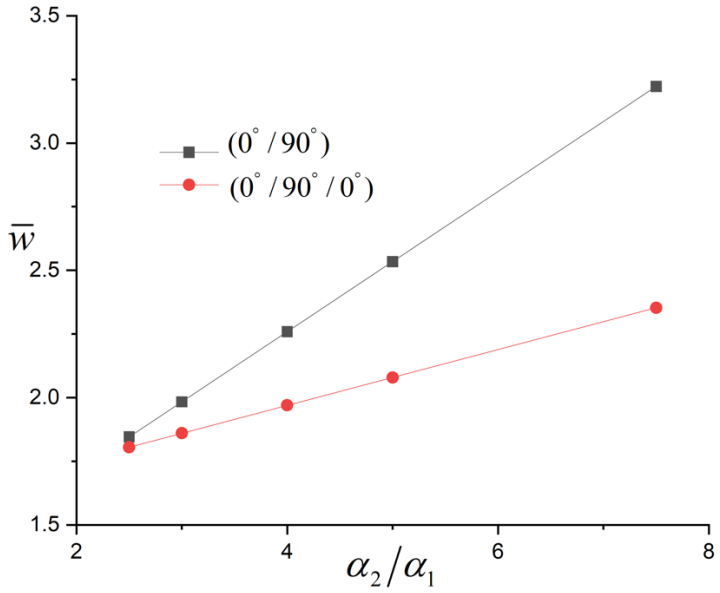

Figure 31:Comparison between thermal expansion coefficient ratio of (0°/90°)Laminate and (0°/90°/0°)Laminate using Present theory

To assess the influence of variation in thermal expansion characteristics on bending behavior, the thermal expansion coefficient ratio α_2/α_1 was varied while maintaining a constant aspect ratio a/h = 10. The variation of non-dimensional deflection $\overline{w}$ with α_2/α_1 was analyzed for [0°/90°] and [0°/90°/0°] laminates using the present theory, the trigonometric theory (Ghugal & Kulkarni, 2013), and the Higher-Order Shear Deformation Theory (HSDT).

For the [0°/90°] laminate (Figure 29), all three theories produced identical results, showing a clear increase in $\overline{w}$ as α_2/α_1 increased. A similar trend was observed for the [0/90/0] laminate (Figure 30), where the three theories again yielded consistent and similar results. This behavior reflects the greater thermal strain in the transverse direction as α_2 becomes larger relative to α_1, inducing more bending deformation.

A comparison between the two laminates using the present theory revealed that the [0°/90°] configuration consistently exhibited higher deflection than the [0°/90°/0°] laminate. This is attributed to the additional outer 0° plies in the [0°/90°/0°] laminate, which enhance bending stiffness and reduce deformation. While both laminates follow the same general trend, the difference in slope indicates varying sensitivity to uneven thermal expansion. These results confirm that the present theory effectively captures thermal expansion effects in cross-ply laminates.

4.4. Conclusion

In this chapter, a detailed numerical investigation was conducted to evaluate the bending response of cross-ply laminated plates under thermal loading using the present refined displacement theory. Comparative analyses with Classical Plate Theory (CPT), First-Order Shear Deformation Theory (FSDT), Higher-Order Shear Deformation Theory (HSDT), and the Trigonometric theory (Ghugal & Kulkarni, 2013) confirmed the accuracy and consistency of the present theory, especially in capturing transverse shear and thermal effects.

Results showed excellent agreement between the present theory, HSDT, and the trigonometric theory across various laminate configurations and aspect ratios. Parametric studies further demonstrated expected trends: deflection increased with increasing aspect ratio a/h for [0°/90°] laminates, while it decreased for [0°/90°/0°], and decreased with increasing material anisotropy ratio E_1/E_2, while it increased with rising thermal expansion coefficient ratio α_2/α_1. These findings validate the applicability of the present theory for accurate modeling of laminated composite plates subjected to thermal load.

It was observed that for [0°/90°] laminates, deflection increased with aspect ratio, while for [0°/90°/0°], it decreased.

GENERAL CONCLUSION

The use of laminated composite plates in structural engineering is of critical importance due to their high strength-to-weight ratio and resistance to environmental and mechanical stresses. These materials are widely applied across several high-performance industries, including aerospace, automotive, marine, civil, and military engineering, where advanced structural behavior and reliability are essential; and they are often exposed to severe thermal environments. Consequently, the accurate modeling and analysis of their thermal responses remain a vital area of research.

In this work, a refined shear deformation theory has been developed and applied to the static analysis of cross-ply laminated composite plates subjected to thermal loading. The proposed theory incorporates a higher-order transverse shear deformation formulation, enabling realistic representation of warping effects through the plate thickness without the need for shear correction factors. This approach aligns with the class of high-order theories (HSDT) and provides a more accurate prediction of deflections and internal stresses, particularly in moderately thick and thick laminate configurations.

Validation of the present theory was carried out through detailed comparisons with existing theories, including Classical Plate Theory (CPT), First-Order Shear Deformation Theory (FSDT), Higher-Order Shear Deformation Theory (HSDT), and the trigonometric theory (Ghugal & Kulkarni, 2013). The present model consistently showed close agreement with the higher-order formulations, especially in cases involving thermal gradients and anisotropic behavior.

Parametric studies were performed to investigate the influence of key parameters such as the aspect ratio a/h, material anisotropy ratio E_1/E_2, and thermal expansion coefficient ratio α_2/α_1. The results demonstrated expected and physically consistent trends: deflection decreased with increasing stiffness, while it increased with thermal expansion coefficient ratios. For aspect ratio ,deflection increased with aspect ratio for [0°/90°] laminate, while it decreased with increasing aspect ratio for [0°/90°/0°] laminate. These outcomes further confirm the robustness of the proposed theory in capturing the complex behavior of laminated composites under thermal loading conditions.

Overall, this study underscores the importance of using advanced plate theories in the modeling of composite laminates, particularly when addressing thermal effects. The findings contribute to the ongoing development of accurate and efficient analytical tools for composite structures

and lay a strong foundation for further research into dynamic, nonlinear, or damage-based analyses using the present refined model.

REFERENCES

1. ACI Committee 440. (2015). Guide for the Design and Construction of Externally Bonded FRP Systems for Strengthening Concrete Structures.
2. Allix, O. (1989). Méthodes asymptotiques pour les structures composites. PhD Thésis, École Normale Supérieure de Cachan.
3. Altenbach, H., & Altenbach, J. (2004). Einführung in die Strukturmechanik: mit Anwendungen. Springer.
4. Altenbach, H., & Altenbach, J. (2004). Introduction to Continuum Mechanics for Engineers. Springer.
5. Altenbach, H., & Altenbach, J. (2004). Introduction to the Mechanics of Composite Materials.
6. Altenbach, H., & Altenbach, J. (2010). Introduction to Continuum Mechanics for Engineers. Springer.
7. Altenbach, H., & Kissing, W. (2005). Strukturmechanik: Festigkeitslehre mit Anwendungen. Springer.
8. Altenbach, H., Altenbach, J., & Kissing, W. (2015). Mechanics of Composite Structural Elements. Springer.
9. Altenbach, H., Kissing, W., & Öchsner, A. (2013). Metal Matrix Composites. Springer.
10. Ashby, M. F. (2011). Materials Selection in Mechanical Design.
11. Baker, A., Dutton, S., & Kelly, D. (2004). Composite Materials for Aircraft Structures.
12. Berdichevsky, V. L. (1990). Variational-asymptotic method of constructing a theory of shells. Journal of Applied Mathematics and Mechanics, 54(5), 718–735.
13. Berdichevsky, V. L. (1999). Variational-asymptotic method of constructing a theory of shells. PMM Journal of Applied Mathematics and Mechanics, 63(1), 105–113.
14. Berthelot, J. M. (1999). Composite Materials: Mechanical Behavior and Structural Analysis.
15. Brigante, D. (2011). Composite Materials: Properties, Characterisation and Applications. Momentum Press.
16. Brigante, D. (2011). Engineering materials: Research, applications, and advances. Momentum Press.
17. Brigante, D. (2014). Composite Materials Engineering.

18. Brigante, D. (2014). Engineering & Design of Composite Materials. Engineering Books Press.
19. Callister, W. D., & Rethwisch, D. G. (2014). Materials Science and Engineering: An Introduction (9th ed.). Wiley.
20. Carrera, E. (2002). Theories and finite elements for multilayered plates and shells: A unified compact formulation with numerical assessment and benchmarking. Archives of Computational Methods in Engineering, 9(2), 87–140.
21. Carrera, E. (2003). Historical review of zig-zag theories for multilayered plates and shells. Applied Mechanics Reviews, 56(3), 287–308.
22. Carrera, E., & Petrolo, M. (2011). Refined layer-wise models for laminated composite plates. Composite Structures, 93(6), 1570–1583.
23. Carrera, E., Cinefra, M., Petrolo, M., & Zappino, E. (2011). Finite Element Analysis of Structures through Unified Formulation. Wiley.
24. Chawla, K. K. (2012). Composite Materials: Science and Engineering.
25. Chung, D. D. L. (2010). Composite Materials: Science and Applications (2nd ed.). Springer.
26. Clyne, T. W., & Withers, P. J. (1993). An Introduction to Metal Matrix Composites. Cambridge University Press.
27. Cowper, G. R. (1966). The shear coefficient in Timoshenko beam theory. Journal of Applied Mechanics, 33(2), 335–340.
28. Daniel, I. M., & Ishai, O. (2006). Engineering Mechanics of Composite Materials.
29. Di Sciuva, M. (1986). A zig-zag model for multilayered plates. Composite Structures, 6(1), 43–59.
30. Du, S. (2002). High-performance polymeric materials and their composites. Chemical Industry Press.
31. Du, S., & Zhang, L. (2000). High-Performance Polymer Matrix Composites. Chinese Journal of Materials Science.
32. Du, S., & Zhang, L. (2013). Ceramic Matrix Composites and Fiber–Matrix Interfaces.
33. Dutton, S., & Kelly, D. (1998). Introduction to Composite Materials and Structures. Engineering Materials Series.
34. Dutton, S., & Kelly, D. (2004). Introduction to composite materials and structures. Engineering Materials Series.
35. Dutton, S., Kelly, D., & Baker, A. (2004). Composite Materials for Aircraft Structures.

36. Fish, J., & Yu, Q. (2001). Multiscale finite element method for a locally nonperiodic microstructure. International Journal for Numerical Methods in Engineering, 52(3), 673–692.
37. Foreman, C. (2005). Advanced Composite Materials and Their Applications. Materials Engineering Press.
38. Foreman, C. (2011). Engineering Materials Technology.
39. Gay, D., & Hoa, S. V. (2007). Composite Materials: Design and Applications.
40. Gibson, R. F. (2016). Principles of Composite Material Mechanics (4th ed.). CRC Press.
41. Harris, B. (1999). Engineering Composite Materials. The Institute of Materials.
42. Herakovich, C. T. (1997). Mechanics of Fibrous Composites. Wiley.
43. Herakovich, C. T. (1998). Mechanics of Fibrous Composites.
44. Herakovich, C. T. (1998). Mechanics of fibrous composites. Wiley.
45. Hollaway, L. C. (2010). Advanced Fibre-Reinforced Polymer (FRP) Composites for Structural Applications.
46. Jones, R. M. (1999). Mechanics of Composite Materials (2nd ed.). Taylor & Francis.
47. Jones, R. M. (2013). Mechanics of Composite Materials.
48. Kaw, A. K. (2005). Mechanics of Composite Materials.
49. Kaw, A. K. (2006). Mechanics of Composite Materials (2nd ed.). CRC Press.
50. Kissing, W. (2003). Werkstoffe: Grundlagen, Verarbeitung, Anwendung. Carl Hanser Verlag.
51. Kissing, W. (2010). Metal Matrix Composites: Processing and Mechanical Behavior. Wiley-VCH.
52. Kissing, W., & Dutton, S. (2003). Advanced Analysis of Composite Laminates.
53. Ladeveze, P. (1988). Homogenization of structures with periodic layers. Computational Mechanics, 3(2), 133–150.
54. Leissa, A. W. (1969). Vibration of Plates. NASA SP-160.
55. Love, A. E. H. (1944). A Treatise on the Mathematical Theory of Elasticity. Dover Publications.
56. Mallick, P. K. (2007). Fiber-Reinforced Composites: Materials, Manufacturing, and Design.
57. Miehe, C., & Koch, A. (2002). Computational micro-to-macro transitions of discretized microstructures undergoing small strains. Archive of Applied Mechanics, 72(4–5), 300–317.

58. Mindlin, R. D. (1951). Influence of rotary inertia and shear on flexural motions of isotropic, elastic plates. Journal of Applied Mechanics, 18(1), 31–38.
59. Miracle, D. B. (2005). Metal matrix composites – From science to technological significance. Composites Science and Technology, 65(15–16), 2526–2540.
60. Mouritz, A. P., & Gibson, A. G. (2006). Fire Properties of Polymer Composite Materials.
61. Murakami, H. (1986). Laminated composite plate theory with improved in-plane responses. Journal of Applied Mechanics, 53(2), 361–366.
62. NATO Science Series. (2000). Advanced Materials for Lightweight Structures. IOS Press.
63. NATO Science Series. (2001). Applications of Composite Materials. Kluwer Academic Publishers.
64. NATO Science Series. (2001). Metal matrix composites and their applications. Springer.
65. NATO Science Series. (2003). Advanced Composite Materials for Aerospace Engineering.
66. Nguyen, Q. S. (2004). Mécanique des matériaux composites stratifiés. Hermes Science.
67. Noor, A. K., & Burton, W. S. (1990). Assessment of shear deformation theories for multilayered composite plates. Applied Mechanics Reviews, 43(3), 67–97.
68. Pickering, K. L. (2015). Properties and Performance of Natural-Fibre Composites.
69. Reddy, J. N. (1997). Theory and Analysis of Elastic Plates and Shells (2nd ed.). CRC Press.
70. Reddy, J. N. (2004). Mechanics of Laminated Composite Plates and Shells: Theory and Analysis (2nd ed.). CRC Press.
71. Reissner, E. (1945). The effect of transverse shear deformation on the bending of elastic plates. Journal of Applied Mechanics, 12, A69–A77.
72. Sanchez-Palencia, E. (1980). Non-Homogeneous Media and Vibration Theory. Springer.
73. Strong, A. B. (2008). Fundamentals of Composites Manufacturing: Materials, Methods and Applications (2nd ed.). SME.
74. Surappa, M. K. (2003). Aluminium matrix composites: Challenges and opportunities. Sadhana, 28(1–2), 319–334.

75. Tessler, A., & Di Sciuva, M. (1993). A layerwise theory for laminated composite plates. NASA Technical Paper 3264.
76. Timoshenko, S., & Woinowsky-Krieger, S. (1959). Theory of Plates and Shells. McGraw-Hill.
77. Yi, X. S. (2003). Thermoplastic Matrix Composites: Processing and Mechanical Behavior. Elsevier.
78. Yi, X. S., & Du, S. (2011). Advanced Composites. Tsinghua University Press.
79. Yi, X.-S., & Zhang, L.-T. (2006). Micromechanics in functionally graded composites. Science Press & Springer.
80. Zhang, L. T., & Du, S. (2010). Thermal and Structural Analysis of Composite Materials. National Defense Industry Press.
81. Zhang, L., & Du, S. (2000). Processing and Properties of High-Performance Fibers. Materials Letters.
82. Zhang, L., & Yi, X.-S. (2006). High Performance Composite Structures.
83. NATO Science Series (2003). Advanced Composite Materials for Aerospace Engineering.
84. Yi, X.-S., Du, S., & Zhang, L. (2006). Advanced Composite Materials.
85. Zhang, L. (2009). Structure and Properties of Composites.
86. Mantari, J.L., Oktem, A.S., & Guedes Soares, C. (2012). A new trigonometric shear deformation theory for isotropic, laminated composite and sandwich plates. International Journal of Solids and Structures, 49(1), pp.43–53.
87. Ghugal, Y.M. & Kulkarni, R. (2013). A new trigonometric shear deformation theory for flexure analysis of thick laminated composite plates. Composite Structures, 105, pp.240–252.
88. Mosallam, A.S. (2014). FRP composite bridges: State-of-the-art in materials and systems. Construction and Building Materials, 50, pp.190–202.